WAVE FUNCTION METHODS FOR QUANTUM DOTS IN MAGNETIC FIELD

Sami Siljamäki

Laboratory of Physics
Helsinki University of Technology

Fysiikan laboratorio
Teknillinen korkeakoulu

DISSERTATION 124 (2003)

WAVE FUNCTION METHODS FOR QUANTUM DOTS IN MAGNETIC FIELD

Sami Siljamäki

Laboratory of Physics
Helsinki University of Technology
Espoo, Finland

Dissertation for the degree of Doctor of Science in Technology to be presented with due permission of the Department of Engineering Physics and Mathematics for public examination and debate in Auditorium E at Helsinki University of Technology (Espoo, Finland) on the 26th of September, 2003, at 12 o'clock noon.

Dissertations of Laboratory of Physics, Helsinki University of Technology
ISSN 1455-1802

Dissertation 124 (2003):
Sami Siljamäki: Wave Function Methods for Quantum Dots in Magnetic Field
ISBN 951-22-6698-9 (print)
ISBN 951-22-6704-7 (electronic)

OTAMEDIA OY
ESPOO, 2003

To Elina

Abstract

This thesis investigates the use of wave-function methods for the study of quantum-dot systems. It investigates single dots, using quantum Monte Carlo techniques in a wide range of magnetic field values, and a double-dot system, using the exact-diagonalization method.

The thesis proposes simple yet accurate many-particle wave functions for various angular-momentum and spin states, for both weak and strong magnetic fields. Using these trial wave functions, it evaluates various properties of dots and studies Wigner crystallization and spin polarization for the weak-field limit. For strong magnetic fields, the thesis investigates ground states of different spin polarizations as a function of the magnetic field and tests the commonly used lowest-Landau-level approximation. The results are compared to calculations from the density-functional theory.

Finally, the thesis presents a method that combines the accuracy of the exact-diagonalization method and the scalability of Monte Carlo methods. The Monte Carlo-based diagonalization is a promising tool for use in situations that cannot be handled with a simple trial wave function, and have too many particles for an exact-diagonalization treatment. For quantum dots, methods for efficiently evaluating the high-magnetic-field basis functions and their gradients are demonstrated.

Preface

I performed the thesis research in the Computational Condensed Matter and Complex Materials Group, at the Laboratory of Physics, of the Helsinki University of Technology, during 1999-2003.

I thank my supervisor, Academy Professor Risto Nieminen, for providing this opportunity and excellent motivation and guidance during the period. I especially express my gratitude to my instructor, Dr. Ari Harju for his considerable contribution, and for helping me advance with new ideas and insights into the physical problems we dealt with. A special recognition goes to Dr. Viktor Sverdlov for the useful and challenging discussions, and for the long-term collaboration. I also thank Henri Saarikoski, Esa Räsänen, Petteri Hyvönen, Prof. Martti Puska, and Prof. Juhani von Boehm for the collaboration and inspiring discussions. I acknowledge the current and former members of the Laboratory of Physics for creating a nice working environment, especially Tuomas Torsti, Juha Lento, Meri Marlo, Ivan Degtyarenko, and Eija Järvinen.

I am deeply grateful to my wife Elina, for sharing all the pleasant and unpleasant moments, and always providing me with support and joy.

Finally, I acknowledge the National Graduate School in Materials Physics and Vilho, Yrjö and Kalle Väisälä Foundation for their financial support.

Espoo, May 2003

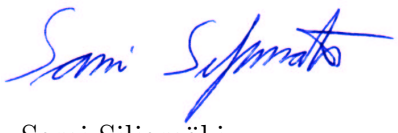

Sami Siljamäki

Contents

List of Publications

This thesis consists of an overview and the following publications:

I A. Harju, S. Siljamäki, and R. M. Nieminen: *Wave function for quantum-dot ground states beyond the maximum-density droplet*, Physical Review B **60**, 1807 (1999).

II S. Siljamäki, V. A. Sverdlov, A. Harju, P. Hyvönen and R. M. Nieminen: *Stability of the maximum-density droplet state in quantum dots: a quantum Monte Carlo study*, Physica B **284–288**, 1776 (2000).

III A. Harju, S. Siljamäki, and R. M. Nieminen: *Two-Electron Quantum Dot Molecule: Composite Particles and the Spin Phase Diagram*, Physical Review Letters **88**, 226804 (2002).

IV A. Harju, S. Siljamäki, and R. M. Nieminen: *Wigner molecules in quantum dots: A quantum Monte Carlo study*, Physical Review B **65**, 075309 (2002).

V H. Saarikoski, E. Räsänen, S. Siljamäki, A. Harju, M. J. Puska, and R. M. Nieminen: *Electronic properties of model quantum-dot structures in zero and finite magnetic fields*, The European Physical Journal B **26**, 241 (2002).

VI S. Siljamäki, A. Harju, R. M. Nieminen, V. A. Sverdlov, and P. Hyvönen: *Various spin-polarization states beyond the maximum-density droplet: A quantum Monte Carlo study*, Physical Review B **65**, 121306(R) (2002).

The author has had an active role in all the phases of the research reported in this thesis. He is responsible for several developments in variational quantum Monte Carlo calculations, reported in Publications I, II, IV, and VI. He wrote Publications II and VI and is the main responsible for developing numerical algorithms, and performing calculations and analyses for Monte Carlo-based diagonalization methods. The author calculated the single-dot quantum Monte Carlo results presented in Publication V.

Chapter 1

Introduction

An increasingly large portion of modern condensed-matter science concentrates on man-made structures. Advances in recent decades in manufacturing technology and experiments have decreased the gap between the atomic and bulk regimes and given rise to mesoscopic physics between the two extremes. This new field has raised fundamental physical questions, many of which are still unresolved. Nonetheless, simple applications, like ordinary laser diodes, are already widespread.

Theoretically, mesoscopic structures provide a wealth of intriguing challenges, especially in low-dimensional systems. In atoms, for example, the strong and massive nucleus obscures much of the effects of interactions, whereas in mesoscopic structures, interactions between charge carriers play an important role. The strong interactions result in a highly correlated state of charge carriers, to which single-particle theories are no longer valid. Perhaps the most famous examples of such new states of matter are integer and fractional quantum Hall effects [1–3], observed in magnetic fields.

Solving the state of an *interacting* N-electron system requires solving the N-particle Schrödinger equation

$$\mathsf{H}\Psi = E\Psi\,,$$

where Ψ is the wave function of all particles, H is the Hamiltonian operator, and E is the total energy. Solving this equation analytically is possible in special cases only, and solving it numerically is almost as difficult: already the general case of two-particles in two dimensions, giving four degrees of freedom, is challenging. For increasing degrees of freedom, it soon becomes utterly impossible to just store the numerical values of the wave function (on a grid of reasonable spacing) in a computer's memory space.

It is possible to get past the difficulties in solving the interacting Schrödinger equation. Because the difficulties emerge from interactions, various mean-field theories take the interactions into account only in an averaged way. The widely used density-functional theory [4] and the Hartree-Fock methods belong to this class.

With increasing computational power, methods solving the wave function exactly have become increasingly popular. These methods treat interaction effects accurately. The exact-diagonalization method aims at solving the Schrödinger equation to a point of numerical accuracy, by using a suitably chosen basis set. The number of particles is, however, severely limited by the rapidly increasing basis size. Various Monte Carlo methods [5], on the other hand, use a statistical approach, which is in principle accurate, and can be applied in some cases to systems containing up to several thousand particles.

1.1 Quantum dots

Quantum dots are fabricated, nanoscale structures, which are able to capture and localize charge carriers, such as electrons. Typical dimensions for quantum dots range from nanometers to a few micrometers, and the number of electrons can be tuned from zero to up to thousands.

Quantum dots resemble ordinary atoms in many ways. Both contain a more or less fixed number of electrons, have a shell structure, and even the experimental Hund's rule describing the spin alignment in atomic shells also holds for quantum dots in many cases [6, 7]. These similarities gave rise to the term "artificial atom", which is commonly used as a synonym for quantum dot.

Quantum dots are much larger than real atoms. From the technological point of view, however, the most important difference between quantum dots and atoms is that the properties of quantum dots can be tailored by design, or even in real time, by adjusting the electromagnetic environment of the dot. This opens a broad spectrum of new possibilities, ranging from superior laser technology [8, 9] to applications of quantum-dot transistor [10] or memory technologies [11], and even future applications in quantum computing [12, 13].

For a theoretician, quantum dots are interesting objects. As highly correlated many-particle systems, with tunable properties, they are excellent for studies of electron-electron interactions. Spin effects are also pronounced

in quantum dots: the magnetic field needed to produce spin effects of similar magnitude in atoms is millions of times higher than in quantum dots. For small quantum dots, complete spin polarization can be easily achieved in laboratories.

Quantum dots can be manufactured in a number of different ways. Vast quantum-dot arrays can be created using various self-assembly methods [14–16] or, for example, by cluster deposition [17]. Both metallic [see Fig. 1.1(a)] and semiconductor dot arrays can be made. A few dots or molecules can be also created by using a scanning tunneling microscope. It is possible to make the self-organized dots in the arrays extremely small, but the height of the dots is typically of the same order as their diameter, which makes them three-dimensional.

Two-dimensional quantum dots can be manufactured at semiconductor interfaces, which have a quasi-two-dimensional electron gas (2DEG) in the inversion layer. Electrodes, which create the confining electrostatic potential and contacts to the dot, can be made with lithographic techniques on top of the structure, thereby producing lateral dots [see Fig. 1.1(d)]. By etching away most of the 2DEG interface, vertical semiconductor dots [see Fig. 1.1(b,c)] can be created. Vertical dots are typically smaller than lateral dots, down to the size of a single-electron dot.

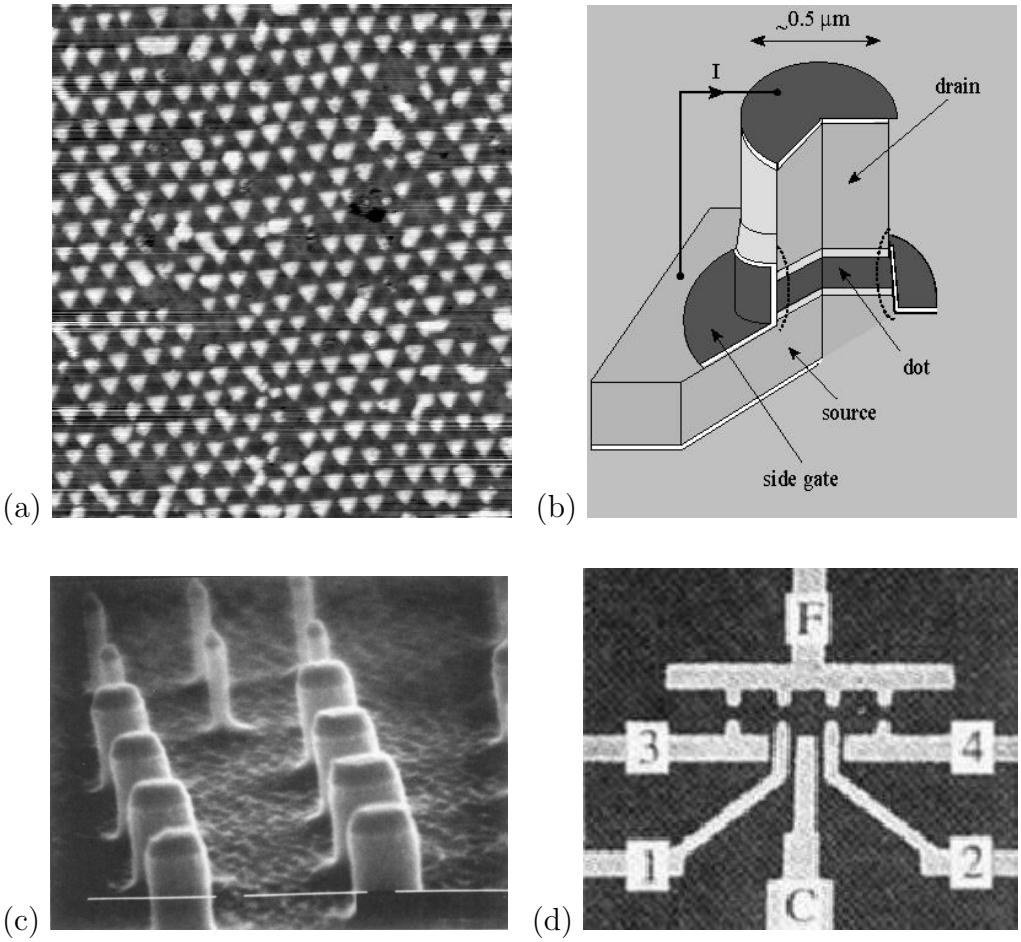

Figure 1.1: (a): An array of self-organized Fe quantum dots on dislocation network of Cu bilayer on Pt(111) surface. The size of each dot is approximately 4 nm (from Ref. 14 by H. Brune et al.). (b): A schematic figure of a vertical quantum dot (from Ref. 18 by L. Kouwenhoven and C. Marcus). (c): Experimental realizations of vertical GaAs quantum dots. Horizontal bars are 0.5 μm (from Ref. 19 by M. A. Reed et al.). (d): A lateral quantum dot on top of GaAs/AlGaAs heterostructure. The effective size of the dot in the center of the structure is approximately 800 nm. (from Ref. 20 by L. P. Kouwenhoven et al.).

Chapter 2

Monte Carlo methods

Monte Carlo (MC) methods are a broad collection of techniques to gather information from complex systems. The formulation of the problem is usually as follows: evaluate the average value of some quantity over all possible states of the system. If the number of states is so large that it is impossible to handle all, or even a subset of them, in any systematic way, then MC methods may prove to be the best or the only choice. In an MC method, only a small but representative random subset of all states is selected, and the size of the subset can be chosen at will. As an example, an MC method might be used to simulate the average waiting time for a lift in a high building to optimize the driving logic.

Systems often have a natural time evolution. In MC methods, any such complex time dependence or dynamics is replaced by "stochastic dynamics" from random numbers. The system is transferred to a new state, completely ignoring the real time evolution between initial and final states. This makes the MC method powerful, but also limited in measuring dynamical properties on a quantitative (real-time) level.

2.1 Monte Carlo integration

Monte Carlo integration is an integration method with random sample points [21, 22]. Using the terms from the last section, the set of states would correspond to the set of all numbers in the volume of integration. In traditional methods, like the Simpson's method, the integrand is evaluated at each point on a regular quadrature. If the volume is very high dimensional, then it is impossible to even go through all the quadrature points in

a reasonable time (if there is more than one point per dimension). In the MC integration, the number of sample points can be chosen freely. Another advantage of the MC integration is that it can be easily implemented in almost any geometry: infinite regions or fractals cause no problems.

The MC integration method is based on the following limit:

$$\frac{1}{M}\sum_{i=1}^{M} f(\mathbf{R}_i) \xrightarrow[M\to\infty]{} \frac{1}{V}\int_V f(\mathbf{R})\, d\mathbf{R}\,, \tag{2.1}$$

where points $\mathbf{R}_i$ are uniformly randomly distributed throughout the volume of integration V. The error term is statistical, and decays as

$$e \propto \frac{\sigma}{\sqrt{M}}\,, \tag{2.2}$$

where σ is the standard deviation of the integrand and M the number of sample points. The major advantage in this kind of an error term is the independence on the dimensionality d of the space. In traditional methods, the error estimate deteriorates as the dimensionality increases: for example, the error in the trapezoidal method behaves like $e \propto M^{-2/d}$ and in the Simpson's method like $e \propto M^{-4/d}$. For large d, the MC integration becomes superior to most quadrature methods.

2.1.1 Importance sampling

If the integrand is highly peaked, the standard deviation σ in Eq. (2.2) is large. This is often the case in physical applications involving many-dimensional integrals, and it makes the direct use of Eq. (2.1) inefficient. The following transformation can be used to reduce the variance:

$$\frac{1}{M}\sum_{i=1}^{M} f(\mathbf{R}_i) = \frac{1}{M}\sum_{i=1}^{M} p(\mathbf{R}_i)\frac{f(\mathbf{R}_i)}{p(\mathbf{R}_i)} \sim \frac{I_p}{M}\sum_{i=1}^{M}\frac{f(\mathbf{R}_i^p)}{p(\mathbf{R}_i^p)}\,, \tag{2.3}$$

where $p(\mathbf{R})$ is a positive weight function on V, $I_p = \int_V p(\mathbf{R})\, d\mathbf{R}$, and points $\mathbf{R}_i^p$ are distributed as p. The last two summations are equal in the limit $M \to \infty$. By choosing a suitable p that resembles f, the variance of the ratio f/p can be made significantly lower than the variance of f itself. This is the importance sampling method.

As a consequence of the reduced variance, an additional integral I_p appears in Eq. (2.3). The function p should be chosen so that I_p is calculable.

In some cases (see Sec. 2.2), the integral I_p cancels out from the final result, and its value is not needed at all.

Besides the reduction of the variance, the importance sampling can be used to directly evaluate integrals over infinite volumes, since uniformly distributed random numbers for Eq. (2.1) can only be generated for finite volumes. For these applications, one should be careful about the liming behavior of p with respect to f.

2.1.2 Metropolis algorithm

Generating *independent* random points from a many-dimensional p is generally difficult. Direct methods are available only for a few special cases. Correlated random points, however, are easy to generate as a path in a Markov chain. The states in the chain are exactly the states of the system being simulated, and the transition probabilities between states are given by a stochastic matrix.[1]

Let $\boldsymbol{\pi}$ be the stochastic matrix for the Markov chain. The matrix $\boldsymbol{\pi}$ determines the unique limiting distribution for the chain (if such exists), but in this case the inverse problem needs to be solved: how to construct the matrix $\boldsymbol{\pi}$ from the known distribution p? Among many solutions, the "asymmetric rule" by Metropolis et al. [23] is perhaps the most widely used:

$$\pi_{nm} = \tau_{nm} \min\left(1, \frac{p_m}{p_n}\right) . \tag{2.4}$$

Here $\boldsymbol{\tau}$ is any symmetric matrix with diagonal elements $\tau_{nn} = 1 - \sum_{m \neq n} \pi_{nm}$. The element τ_{nm} gives the probability of *selecting* the next trial state to be the state m. The actual acceptance probability is then determined from the ratio p_m/p_n. As the number of points $\mathbf{R}^p$ generated from Eq. (2.4) approaches infinity, the distribution of points approaches p.

The random points from the Metropolis algorithm are correlated. Each state depends on the previous one, and the amount of correlation is determined by the matrix $\boldsymbol{\tau}$. If only near-by states can be selected, then correlations are large, but if any state in the system can be selected with equal probability, correlations are small (but not zero). The optimal $\boldsymbol{\tau}$ depends on the application. A common rule of thumb for a variational quantum Monte Carlo simulation is that about half of the trial states should be accepted,

[1] π_{nm} gives the transition probability from state n to state m given that the system is in state n. The row sums of $\boldsymbol{\pi}$ are 1.

but to properly minimize the error term, the optimal $\boldsymbol{\tau}$ should be searched separately in each case.

Autocorrelation

The autocorrelation function can be used to measure the degree of correlations in the Markov chain. Let $f(\mathbf{R})$ be some property of the system in state $\mathbf{R}$. The correlation coefficient of f between states separated by n steps in the chain, C_n, can be defined as

$$C_n = \frac{\langle f_i f_{i+n} \rangle - \langle f_i \rangle^2}{\langle f_i^2 \rangle - \langle f_i \rangle^2}\,, \tag{2.5}$$

where $f_i = f(\mathbf{R}_i^p)$, and $\langle \cdots \rangle$ is the average value over the whole simulation. The autocorrelation function is normalized so that C_0 is 1.

In practice, calculating the function C_n from Eq. (2.5) is slow. Interpreting C_n as a convolution, and using a Fourier transform $\mathcal{F}$, yields a more useful expression:

$$\tilde{\mathbf{C}} = \mathcal{F}^{-1}\big(|\mathcal{F}\,(\mathbf{f})\,|^2\big)\,, \tag{2.6}$$

$$\mathbf{C} = \frac{1}{\tilde{C}_1}\left[\frac{\tilde{\mathbf{C}}}{N} - \left(\frac{\sum_i f_i}{N}\right)^2\right]\,, \tag{2.7}$$

where $\mathbf{f} = (f_1, f_2, \ldots, f_N)$ and $\mathbf{C} = (C_1, C_2, \ldots, C_N)$. This method is $\mathcal{O}(N \log N)$ while Eq. (2.5) is $\mathcal{O}(N^2)$. In the limit of a long sample vector $\mathbf{f}$, both methods give the same autocorrelation.

The autocorrelation length ξ can be defined as

$$\xi = \sum_n C_n\,. \tag{2.8}$$

To compute the error bounds from Eq. (2.2), which is valid for independent sample points only, the number of sample points should be divided by ξ:

$$e \propto \frac{\sigma}{\sqrt{M/\xi}}\,. \tag{2.9}$$

However, more rigorous error bounds can be obtained by running several independent MC calculations in parallel.

2.2 Variational quantum Monte Carlo

Quantum Monte Carlo methods are tailored to integrate quantum mechanical expectation values, like the ground-state energy. The variational quantum Monte Carlo method (VMC) is perhaps conceptually the simplest one, and is a direct application of the MC integration presented above.

Let Ψ be the wave function of a system of N particles. The expectation value of an operator A in this state is defined as

$$\frac{\langle \Psi \left| \mathsf{A} \right| \Psi \rangle}{\langle \Psi | \Psi \rangle}\,, \tag{2.10}$$

where Ψ need not be normalized. By performing the transformation

$$\frac{1}{\langle \Psi | \Psi \rangle} \int \Psi^* \mathsf{A} \Psi \, d\mathbf{R} = \frac{1}{\langle \Psi | \Psi \rangle} \int |\Psi|^2 \frac{\mathsf{A}\Psi}{\Psi} \, d\mathbf{R}\,, \tag{2.11}$$

the expectation value can be interpreted as an importance-sampling MC integral:

$$\frac{\langle \Psi \left| \mathsf{A} \right| \Psi \rangle}{\langle \Psi | \Psi \rangle} = \left\langle \frac{\mathsf{A}\Psi}{\Psi} \right\rangle_{|\Psi|^2}\,, \tag{2.12}$$

where $\langle \cdots \rangle_p$ means the expectation value with sample points distributed as p. The norm $\langle \Psi | \Psi \rangle$ [denoted I_p in Eq. (2.3)] cancels out. The quantity $(\Psi^{-1}\mathsf{A}\Psi)(\mathbf{R})$ is called the local value of the operator A at $\mathbf{R}$. For an eigenstate of A, it is independent of $\mathbf{R}$ and equal to the corresponding eigenvalue.

According to the variational principle, the energy given by any trial wave function Ψ is an upper bound to the true ground-state energy. This is the corner stone of the VMC method. The variational principle allows one to construct a wave function $\Psi_{\boldsymbol{\alpha}}$ with free variational parameters $\boldsymbol{\alpha} = (\alpha_1, \alpha_2, \ldots, \alpha_n)$, and optimize the form of the wave function by minimizing the expectation value of the local energy,

$$\langle E_L \rangle_{|\Psi_{\boldsymbol{\alpha}}|^2} = \left\langle \frac{\mathsf{H}\Psi_{\boldsymbol{\alpha}}}{\Psi_{\boldsymbol{\alpha}}} \right\rangle_{|\Psi_{\boldsymbol{\alpha}}|^2}\,, \tag{2.13}$$

with respect to the parameters. In principle, if the parametrized function $\Psi_{\boldsymbol{\alpha}}$ spans the whole Hilbert space, then by minimizing the local energy (2.13) the trial wave function converges to the exact quantum mechanical ground state. The special case of a linear variational wave function, in which $\Psi_{\boldsymbol{\alpha}}$ is a linear combination of basis functions with coefficients α_i, leads to a matrix diagonalization problem that will be handled in Ch. 3.

In VMC simulations it is common to minimize the variance of the local energy σ^2 instead of the local energy E_L itself [24, 25]. The reasons for this include numerical stability and the knowledge of the absolute lower bound (zero) of the quantity being minimized. Nevertheless, the minimum of variance need not coincide with the minimum of energy, which is a fundamental problem in all variance-minimization techniques. The methods to be presented below have largely solved the problems with numerical stability, and they have made the variance minimization unnecessary in many cases. In this thesis all minimizations are based on direct energy minimization.

The slowly decaying statistical error ($\propto M^{-1/2}$) present in MC simulations makes the optimization of variational parameters nontrivial. Methods that do not take the noise into account are generally useless, at least near the optimal point. The traditional method of handling the noise in energy minimization is to take a large, fixed set of points $\{\mathbf{R}_i\}$ distributed as $|\Psi|^2$. The parameter optimization is then carried out using some traditional technique within the chosen set of sample points. Since the points are fixed, the energy function $E(\{\mathbf{R}_i\};\boldsymbol{\alpha})$ is an analytic function of $\boldsymbol{\alpha}$ with no noise, and the ordinary minimization works. (This method of the noise elimination is actually the correlated sampling method presented in Sec. 2.3.) The set $\{\mathbf{R}_i\}$ needs to be large, to minimize the statistical error in the position of the minimum, or equivalently, to keep the form of the function $E(\{\mathbf{R}_i\};\boldsymbol{\alpha})$ close to the true energy function $E(\boldsymbol{\alpha})$.

The problem in traditional approaches is that the distribution $\{\mathbf{R}_i\}$ corresponds to the initial parameter set $\boldsymbol{\alpha}_0$, not the current set $\boldsymbol{\alpha}_i$. This causes bias, and the minimum $\boldsymbol{\alpha}^*$ that is found is not the true minimum. A new optimization with an updated set $\{\mathbf{R}_i\}$ can be done, but the recalculation of the sample points is slow because of the large number of configurations.

Stochastic Gradient Approximation

The stochastic gradient approximation (SGA) [26] is a minimization technique that has no bias. In SGA, the number of configurations m is small and the configurations follow the evolution in parameter space. As a result, the noise is not completely eliminated, but only damped more and more as the optimization proceeds. Indeed, this turns out to be one of the strengths of the SGA method.

Let $Q(\boldsymbol{\alpha})$ be the quantity to be minimized with respect to parameters

$\boldsymbol{\alpha}$, e.g., the energy. The SGA method can be summarized in the formula

$$\boldsymbol{\alpha}_{j+1} = \boldsymbol{\alpha}_j - \gamma_{j+1} \nabla_\alpha \left[\frac{1}{m} \sum_i Q(\{\mathbf{R}_i^{(j)}\}; \boldsymbol{\alpha}_j) \right], \tag{2.14}$$

where γ_j is the damping parameter, $\{\mathbf{R}_i^{(j)}\}_{i=1}^m$ is the set of configurations for the iteration number j, and ∇_α is the gradient in the parameter space. As the name suggests, the gradient is a stochastic, unbiased approximation to the real gradient. Even at the minimum $\boldsymbol{\alpha}^*$, the gradient need not be zero, because $Q(\{\mathbf{R}_i^{(j)}\}; \boldsymbol{\alpha}_j)$ does not need to be a very good approximation to the actual $Q(\boldsymbol{\alpha})$. Only in the limit $j \to \infty$ the gradient vanishes.

The damping, determined by γ_j, should satisfy [27] the conditions

$$\sum_j \gamma_j^2 < \infty \quad \text{and} \quad \sum_j \gamma_j = \infty \,. \tag{2.15}$$

The first condition ensures strong enough damping, and the second guarantees that all points can be reached in the parameter space. A choice that satisfies both conditions is $\gamma_j = j^{-r}$, where $\frac{1}{2} < r \leq 1$.

The evaluation of the parameter gradient ∇_α can be done using a finite-difference method and the correlated sampling (see the next section). However, a better method using analytical energy derivatives is presented in Ref. 28. Generalizing this method to complex-valued wave functions it can be written as

$$\frac{\partial}{\partial \alpha_i} \langle E_L \rangle = 2 \,\mathrm{Re} \left\{ \left\langle E_L \frac{\partial \ln \Psi^*}{\partial \alpha_i} \right\rangle - \langle E_L \rangle \left\langle \frac{\partial \ln \Psi^*}{\partial \alpha_i} \right\rangle \right\}, \tag{2.16}$$

where $\langle \cdots \rangle$ denotes the average over the set $\{\mathbf{R}_i^{(j)}\}_{i=1}^m$ and Re takes the real part. Eqs (2.14) and (2.16) together make up a powerful minimization scheme for VMC simulations.

2.3 Correlated sampling

The driving wave function, from which the random points $\mathbf{R}_i^p$ are sampled, can be separated from the wave function whose properties are being solved. Let Ψ_0 be the driving wave function, and let $\{\Psi_i\}_{i \geq 1}$ be a set of some other wave functions. Eq. (2.12) can be generalized to give

$$\frac{\langle \Psi_n | \mathsf{A} | \Psi_m \rangle}{\langle \Psi_0 | \Psi_0 \rangle} = \left\langle \frac{\Psi_n^* \mathsf{A} \Psi_m}{\Psi_0^* \Psi_0} \right\rangle_{|\Psi_0|^2} = \left\langle \omega_n \frac{\mathsf{A} \Psi_m}{\Psi_n} \right\rangle_{|\Psi_0|^2}, \tag{2.17}$$

where $\omega_n = |\Psi_n/\Psi_0|^2$. Using this equation to evaluate the norms of Ψ_i's as well, the properly normalized matrix elements of the operator A can be written as:

$$\frac{\langle \Psi_n | \mathsf{A} | \Psi_m \rangle}{\sqrt{\langle \Psi_n | \Psi_n \rangle} \sqrt{\langle \Psi_m | \Psi_m \rangle}} = \frac{\left\langle \omega_n \frac{\mathsf{A}\Psi_m}{\Psi_n} \right\rangle_{|\Psi_0|^2}}{\langle \omega_n \rangle_{|\Psi_0|^2}^{\frac{1}{2}} \langle \omega_m \rangle_{|\Psi_0|^2}^{\frac{1}{2}}} . \tag{2.18}$$

In order to keep the error bounds reasonable, the driving wave function should resemble the wave functions Ψ_n and Ψ_m.

In the correlated sampling method, the equations presented above are used to evaluate the properties of some wave functions Ψ_i and Ψ_j during a single MC run. The resulting expectation values have similar statistical error components, i.e., they are correlated. This can be used to cancel the error. As an example, the difference

$$\frac{\langle \Psi_i | \mathsf{A} | \Psi_i \rangle}{\langle \Psi_i | \Psi_i \rangle} - \frac{\langle \Psi_j | \mathsf{A} | \Psi_j \rangle}{\langle \Psi_j | \Psi_j \rangle}$$

is much more accurately computed using correlated sampling than using two independent MC simulations (provided that Ψ_i and Ψ_j are similar enough). This property of correlated sampling is essential in parameter minimization and Monte Carlo-based diagonalization (see Sec. 3.2).

2.4 Cusp conditions

The local energy $E_L(\mathbf{R}) = T(\mathbf{R}) + V(\mathbf{R})$, where T is the local kinetic energy and V the local potential energy, is independent of $\mathbf{R}$ for any eigenfunction of the Hamiltonian. Any singularities in V (e.g, due to Coulomb interactions when $\mathbf{r}_i \to \mathbf{r}_j$) are canceled exactly by singularities in T. The analytical conditions for a wave function to fulfill this cancellation at singular points of V are called Kato's cusp conditions [29].

To examine the behavior of T as $\mathbf{r}_i \to \mathbf{r}_j$, it is useful to replace the coordinates $\mathbf{r}_i$ and $\mathbf{r}_j$ with

$$\mathbf{r} = \mathbf{r}_i - \mathbf{r}_j \,, \quad M\mathbf{R} = m_i \mathbf{r}_i + m_j \mathbf{r}_j \,, \tag{2.19}$$

where $M = m_i + m_j$ (for generality, let us use different masses for different particles), and let $\mathbf{r} \to 0$. The gradient is transformed respectively as

$$\nabla_{\mathbf{r}} = \frac{\mu}{m_i} \nabla_{\mathbf{r}_i} - \frac{\mu}{m_j} \nabla_{\mathbf{r}_j} \,, \quad \nabla_{\mathbf{R}} = \nabla_{\mathbf{r}_i} + \nabla_{\mathbf{r}_j} \,, \tag{2.20}$$

where $\mu = m_i m_j/(m_i + m_j)$ is the reduced mass. The total kinetic energy operator becomes:

$$\mathsf{T} = -\sum_k \frac{\hbar^2}{2m_k}\nabla^2_{\mathbf{r}_k} = -\frac{\hbar^2}{2\mu}\nabla^2_{\mathbf{r}} - \frac{\hbar^2}{2M}\nabla^2_{\mathbf{R}} - \sum_{k\,(\neq i,j)} \frac{\hbar^2}{2m_k}\nabla^2_{\mathbf{r}_k}\,. \tag{2.21}$$

Without any knowledge of coordinates other than $\mathbf{r}$, the local kinetic energy $T = \Psi^{-1}\mathsf{T}\Psi$ can diverge in the limit $|\mathbf{r}| \to 0$, either because Ψ approaches zero, or because $\nabla^2_{\mathbf{r}}\Psi$ approaches infinity. The latter can happen at points where the wave function has a discontinuous gradient, e.g., at cusps or kinks.

2.4.1 The general Jastrow-Slater wave function

For the Jastrow-Slater wave function $\Psi = DJ$, where D is a product of up and down-spin Slater determinants, and J is a Jastrow factor describing correlations, the cusp condition has a universal form. To derive the condition it is assumed that J is a positive function of interparticle distances and that the states in the Slater determinant are eigenstates of the single-particle Hamiltonian.

For the simplicity of notation, let $\hbar = 1$, and let all the masses m_k be equal to each other and to the unit mass. The correct factors, as in Eq. (2.21), are restored again at the end of this section. With this simplification, the local kinetic energy for the Jastrow-Slater wave function is

$$\Psi^{-1}\mathsf{T}\Psi = -\frac{1}{2}\left(\frac{\nabla^2 D}{D} + 2\frac{\nabla D\cdot\nabla J}{DJ} + \frac{\nabla^2 J}{J}\right)\,, \tag{2.22}$$

where ∇ is the multidimensional gradient with respect to all degrees of freedom of the system. Because single-particle eigenstates are used, $D^{-1}\nabla^2 D$ is finite (and even a constant), but the behavior of the other two terms as $\mathbf{r}_i \to \mathbf{r}_j$ require more analysis.

If $\mathbf{r}_i$ and $\mathbf{r}_j$ represent identical particles, then $D \to 0$, and all cross terms from Eq. (2.22) could contribute to the divergence of T. However, as $\mathbf{r} = \mathbf{r}_i - \mathbf{r}_j \to \mathbf{0}$, then $\nabla_{\mathbf{r}_k} D \to \mathbf{0}$ $(k \neq i, j)$, and also $\nabla_{\mathbf{R}} D \to \mathbf{0}$. The first limit follows from the fact that $\nabla_{\mathbf{r}_k} D$ still contains a determinant that goes to zero, and the latter from Eq. (2.20) and antisymmetry ($\nabla_{\mathbf{r}_i} D \to -\nabla_{\mathbf{r}_j} D$). Hence, the only cross term that may be divergent as $\mathbf{r} \to 0$, is

$$2\frac{\nabla_{\mathbf{r}} D\cdot\nabla_{\mathbf{r}} J}{DJ} \sim 2\frac{\boldsymbol{\eta}}{\boldsymbol{\eta}\cdot\mathbf{r}}\cdot\frac{\partial_r J}{J}\frac{\mathbf{r}}{r} = \frac{2}{r}\frac{\partial_r J}{J}\,, \tag{2.23}$$

where $\boldsymbol{\eta} = \nabla_r D$ and $\partial_r J = \partial J/\partial r$. The results $D \to \boldsymbol{\eta} \cdot \mathbf{r}$ (see the next section) and $\nabla_r J \to \partial_r J\, \mathbf{r}/r$ (particles i and j are identical) have been used.

If the particles are not identical, their coordinates are in different Slater determinants, and D remains non-zero in the limit $\mathbf{r} \to \mathbf{0}$. As a result, none of the cross terms is divergent for a non-zero J. For notational convenience, the divergence (2.23) is multiplied by the factor k, which is 1 for identical particles, and 0 otherwise.

Another divergence may arise from the Laplacian of the Jastrow factor. A non-zero Jastrow factor $J = J(\{r_{ij}\})$, provided that $\partial_r^2 J$ is not divergent at $r = 0$ and $\partial_r J(r)|_{r=0} \neq 0$, has the following limiting behavior as $\mathbf{r} \to 0$:

$$\frac{\nabla_{\mathbf{r}}^2 J}{J} \sim \frac{(d-1)}{r} \frac{\partial_r J}{J}\,, \tag{2.24}$$

where d is the dimensionality of the $\mathbf{r}$-space. Equations (2.23) and (2.24) now give all the divergent components of the kinetic energy when two particles approach each other.

Combining the kinetic energy with the Coulomb potential, and returning to the unit system of Eq. (2.21), the local energy can be written as:

$$E_L \xrightarrow[\mathbf{r}\to\mathbf{0}]{} -\frac{\hbar^2}{2\mu}\left(k\frac{2}{r}\frac{\partial_r J}{J} + \frac{(d-1)}{r}\frac{\partial_r J}{J}\right) + \frac{q_i q_j}{4\pi\epsilon_0 r}\,. \tag{2.25}$$

For this to remain finite as $\mathbf{r} \to \mathbf{0}$, the following condition must be met:

$$\frac{\partial_r J}{J} = \frac{q_i q_j \mu}{2\pi\epsilon_0 \hbar^2\,(2k+d-1)}\,. \tag{2.26}$$

In a unit system, where the Coulomb potential is written as C/r and $\hbar = 1$, this simplifies to

$$\frac{\partial_r J}{J} = \frac{2\mu C}{2k+d-1}\,, \tag{2.27}$$

which, in the case of two-dimensional electrons, can be further simplified to $\partial_r J/J = C/3$ for parallel spins and $\partial_r J/J = C$ for antiparallel spins.

How does a determinant approach zero?

To derive a proper cusp condition for the Jastrow-Slater wave function, one needs to know the asymptotic behavior of the determinant as $\mathbf{r}_i \to \mathbf{r}_j$.

Let us first consider a general second-order determinant

$$D_2 = \begin{vmatrix} \psi_1(\mathbf{r}_1) & \psi_1(\mathbf{r}_2) \\ \psi_2(\mathbf{r}_1) & \psi_2(\mathbf{r}_2) \end{vmatrix} = \psi_1(\mathbf{r}_1)\psi_2(\mathbf{r}_2) - \psi_2(\mathbf{r}_1)\psi_1(\mathbf{r}_2)\,.$$

Assume now that $\mathbf{r}_2$ is fixed and $\mathbf{r}_1 \to \mathbf{r}_2$. Expanding the functions ψ_1 and ψ_2 in a Taylor series around $\mathbf{r}_2$, and denoting $\mathbf{r} = \mathbf{r}_1 - \mathbf{r}_2$, one has:

$$\begin{aligned} D_2 &= \left[\psi_1(\mathbf{r}_2) + \mathbf{r}\cdot\nabla\psi_1(\mathbf{r}_2) + \tfrac{1}{2}\left(\mathbf{r}\cdot\nabla\right)^2\psi_1(\mathbf{r}_2) + \ldots\right]\psi_2(\mathbf{r}_2) \\ &\quad - \left[\psi_2(\mathbf{r}_2) + \mathbf{r}\cdot\nabla\psi_2(\mathbf{r}_2) + \tfrac{1}{2}\left(\mathbf{r}\cdot\nabla\right)^2\psi_2(\mathbf{r}_2) + \ldots\right]\psi_1(\mathbf{r}_2) \\ &= \left(\psi_2\nabla\psi_1 - \psi_1\nabla\psi_2\right)\cdot\mathbf{r} + \mathcal{O}(|\mathbf{r}|^2)\,, \end{aligned} \tag{2.28}$$

where the functions are evaluated at $\mathbf{r}_2$. The factor $\psi_2\nabla\psi_1 - \psi_1\nabla\psi_2$ is a function of $\mathbf{r}_2$ only, and generally a nonzero vector. Specifically, it cannot depend on $\mathbf{r}$, and therefore

$$D_2 \xrightarrow[\mathbf{r}_1\to\mathbf{r}_2]{} (\text{const. vector})\cdot(\mathbf{r}_1 - \mathbf{r}_2)\,, \tag{2.29}$$

irrespective of the exact form of functions ψ_1 and ψ_2. Only in special cases, where $\psi_2\nabla\psi_1 - \psi_1\nabla\psi_2$ is zero at $\mathbf{r}_2$, can the limiting behavior be of higher order than linear.

The full N-row Slater determinant D can now be written as follows:

$$\begin{aligned} D &= \sum_{\sigma}(-1)^{P(\sigma)}\psi_{\sigma_1}(\mathbf{r}_1)\psi_{\sigma_2}(\mathbf{r}_2)\ldots\psi_{\sigma_N}(\mathbf{r}_N) \\ &= \sum_{\sigma_1,\sigma_2}\Big[(-1)^{P(\sigma)}\psi_{\sigma_1}(\mathbf{r}_1)\psi_{\sigma_2}(\mathbf{r}_2)\sum_{\substack{\sigma_3,\ldots,\sigma_N \\ (\neq\sigma_1,\sigma_2)}}\psi_{\sigma_3}(\mathbf{r}_3)\ldots\psi_{\sigma_N}(\mathbf{r}_N)\Big] \\ &= \sum_{i<j}\left\{\left[\psi_i(\mathbf{r}_1)\psi_j(\mathbf{r}_2) - \psi_j(\mathbf{r}_1)\psi_i(\mathbf{r}_2)\right]F_{ij}(\mathbf{r}_3,\mathbf{r}_4,\ldots,\mathbf{r}_N)\right\}, \end{aligned}$$

where F_{ij}'s are some functions, independent of $\mathbf{r}_1$ and $\mathbf{r}_2$, σ is a permutation, and $P(\sigma)$ its parity. Using the result derived above, this can be further simplified,

$$D \xrightarrow[\mathbf{r}_1\to\mathbf{r}_2]{} (\mathbf{r}_1 - \mathbf{r}_2)\cdot\sum_{i<j}\left\{\left[\psi_i(\mathbf{r}_2)\nabla\psi_j(\mathbf{r}_2) - \psi_j(\mathbf{r}_2)\nabla\psi_i(\mathbf{r}_2)\right]F_{ij}(\mathbf{r}_3,\ldots,\mathbf{r}_N)\right\},$$

and since the summation does not contain $\mathbf{r}_1$, it generally follows that for the N-row determinant,

$$D \xrightarrow[\mathbf{r}_i\to\mathbf{r}_j]{} (\text{const. vector})\cdot(\mathbf{r}_i - \mathbf{r}_j)\,. \tag{2.30}$$

As earlier, by suitably choosing $\mathbf{r}_j$ and the functions ψ_i, it is possible to construct higher order zeros as special cases.

The comparison of Eq. (2.30) with the Taylor expansion of D at $\mathbf{r}_j$ shows that the constant vector must be the gradient $\nabla_i D$ evaluated at $\mathbf{r}_j$.

Chapter 3

Diagonalization

It is possible to solve the Schrödinger equation in a numerically exact way for small systems. This can be done by choosing a finite-dimensional subspace of the full infinite-dimensional Hilbert space, and solving the eigenvalues and eigenvectors (i.e. *diagonalizing*) of the Hamiltonian exactly in that subspace. The method is exact in the sense that at the theoretical level there are no approximations: by increasing the basis size, the numerical solution converges to the exact quantum mechanical solution.

Let $\{|\Psi_i\rangle\}$ N_B-dimensional subspace of the full Hilbert space. The eigenvalue equation for a Hermitian operator A in this subspace,

$$\mathsf{A}\,|\Phi_i\rangle = a_i\,|\Phi_i\rangle\ , \tag{3.1}$$

can be written in this basis as a generalized $N_B \times N_B$ matrix eigenvalue equation

$$\mathbf{AC} = \mathbf{SCD}\,, \tag{3.2}$$

where $A_{ij} = \langle\Psi_i\,|\mathsf{A}|\,\Psi_j\rangle$, $S_{ij} = \langle\Psi_i|\Psi_j\rangle$, $\mathbf{C}$ is an unknown matrix of eigenvectors, $|\Phi_i\rangle = \sum_j C_{ji}\,|\Psi_j\rangle$, and $\mathbf{D}$ is an unknown diagonal matrix of the corresponding eigenvalues a_i. Using the orthonormalization condition $\langle\Phi_i|\Phi_j\rangle = \delta_{ij}$, the problem can be formulated as

$$\mathbf{C}^{\mathrm{H}}\mathbf{AC} = \mathbf{D} \qquad \text{and} \qquad \mathbf{C}^{\mathrm{H}}\mathbf{SC} = \mathbf{I}\,. \tag{3.3}$$

Because $\mathbf{A}$ is Hermitian, the system has always a solution. Furthermore, the solution is unique if all the eigenvalues a_i are distinct.

Eq. (3.1) is equivalent to the requirement that $\langle\Phi_i\,|\mathsf{A}|\,\Phi_i\rangle\,/\,\langle\Phi_i|\Phi_i\rangle$'s are stationary against variations in Φ_i. For the Hamiltonian operator, which is bounded from below, this connection extends to the variational principle for the ground state (see Sec. 2.2): not only is the expectation value stationary

for the ground state, but also the minimum value. For the restricted system (3.2) or (3.3), a similar result is the Hylleraas-Undheim theorem [30, 31], which states that also for the excited states, the eigenenergies are upper bounds to the real energies.

The error resulting from the finite basis size can be estimated by performing several diagonalizations with different basis sizes. In an MC-based diagonalization, there is an additional statistical error component, which often outweighs the finite-basis error.

For the numerical process of solving Eq. (3.3), there are efficient routines readily available. The operation count for the diagonalization of a general matrix is $\mathcal{O}(N_B^3)$, but for special cases much faster methods exist. For two-dimensional systems, an important simplification is available in the case of circularly symmetric potentials, where the diagonalization of the Hamiltonian can be done separately in each angular-momentum subspace.

3.1 Exact diagonalization

In the exact-diagonalization method, the Schrödinger equation is solved numerically in as large a Hilbert subspace as possible. The basis $\{|\Psi_i\rangle\}$ is usually chosen to be either determinants of suitable single-particle states, or (at least for small systems) simple functions, so that an analytical treatment can be pursued as far as possible. In the former case, the elements of the interaction Hamiltonian H_{int} are usually not completely analytically calculable, even though the complexity of integrals can be significantly brought down by analytical techniques. In the latter case, even the interaction Hamiltonian may be analytically evaluated, as is done in Publication III.

3.2 Quantum Monte Carlo-based diagonalization

In exact-diagonalization studies, the size of the basis set needed for a good convergence increases very quickly as the number of the degrees of freedom increases. This quickly renders the method useless. Large basis sets are needed because the form of basis functions in exact-diagonalization studies is often dictated by analytical convenience, and as a result they may not correspond very well to the physical system under study. As an example, while it is true that infinite linear combinations of Slater determinants span

the whole many-body Hilbert space, the number of such determinants to reach a satisfactory accuracy for a strongly correlated state can be enormous. A more tailored basis set would allow one to get useful results with fewer basis functions, but such sets might be analytically heavy or unmanageable. This restriction can be overcome by using the quantum Monte Carlo-based diagonalization method (MCD).

In the MCD method, all matrix elements needed in the diagonalization procedure, $\langle \Psi_i | \mathsf{A} | \Psi_j \rangle$ and $\langle \Psi_i | \Psi_j \rangle$, are evaluated during a single QMC simulation. This is accomplished by choosing a suitable driving wave function Ψ_0, and using Eq. (2.17). The common normalization factor $\langle \Psi_0 | \Psi_0 \rangle$ cancels out from Eq. (3.3), and no norms of wave functions are needed.

A disadvantage of the MCD method is that, in addition to the finite-basis error, there will also be statistical errors in the matrix elements. The correlated sampling method (see Sec. 2.3) itself introduces some statistical error to the elements (compared to independent calculations for each of the elements) through the factors ω_i [see Eq. (2.17)], but it also ensures that the total errors in all elements are highly correlated. This common error is, to a large extent, canceled in the diagonalization phase, and in fact the correlated sampling method is superior to independent evaluations of each of the matrix elements. The driving wave function Ψ_0 should resemble the basis functions as much as possible and, e.g., the variational parameters common to all the basis functions should be optimized for the state for which the greatest accuracy is desired.

3.2.1 Hamiltonian matrix elements

In the diagonalization of the Hamiltonian, it is possible to use Eq. (2.17) directly. However, for the commonly used Jastrow-Slater wave function (see Sec. 2.4.1) the analytical evaluation of the $\nabla^2 J$ term may become computationally dominating. In Ref. 32 it is shown how this term can be cast into a more efficient form if J is real and common for all the basis functions. In this section the result is generalized for complex J's in such a way that each basis function can have its own J_i.

Let us write the basis functions as products, $\Psi_i = \Phi_i J_i$, for which the following condition holds:

$$\mathsf{H}\Psi_i = \mathsf{H}(\Phi_i J_i) = J_i \, \mathsf{H}\Phi_i - \nabla\Phi_i \cdot \nabla J_i + \Phi_i \left(-\tfrac{1}{2} \nabla^2 J_i \right) , \qquad (3.4)$$

where ∇ is the gradient with respect to all the degrees of freedom. For the Hamiltonian used in this work [see Eq. (4.1)], this requirement is equivalent

to J_i being an eigenfunction of the total angular-momentum operator with zero eigenvalue: $\mathsf{L}_z(\Phi_i J_i) = J_i \mathsf{L}_z \Phi_i$. The Hamiltonian matrix element from Eq. (2.17) is therefore

$$\begin{aligned} H_{ij} = \tfrac{1}{2}(H_{ij} + H^*_{ji}) =& \frac{1}{2}\left\langle \frac{\Psi_i^*}{{\Psi_0}^*} \cdot \frac{\mathsf{H}\Psi_j}{\Psi_0} \right\rangle_{|\Psi_0|^2} + \frac{1}{2}\left\langle \frac{\Psi_j}{\Psi_0} \cdot \frac{\mathsf{H}\Psi_i^*}{{\Psi_0}^*} \right\rangle_{|\Psi_0|^2} \\ =& \quad \frac{1}{2}\left\langle \frac{J_i^* J_j \left(\Phi_i^* \mathsf{H} \Phi_j + \Phi_j \mathsf{H} \Phi_i^*\right)}{|\Psi_0|^2} \right\rangle_{|\Psi_0|^2} \\ & - \frac{1}{2}\left\langle \frac{\Phi_i^* \nabla \Phi_j \cdot J_i^* \nabla J_j + \Phi_j \nabla \Phi_i^* \cdot J_j \nabla J_i^*}{|\Psi_0|^2} \right\rangle_{|\Psi_0|^2} \\ & - \frac{1}{4}\left\langle \frac{\Phi_i^* \Phi_j \left(J_i^* \nabla^2 J_j + J_j \nabla^2 J_i^*\right)}{|\Psi_0|^2} \right\rangle_{|\Psi_0|^2} . \end{aligned} \tag{3.5}$$

Let I_{H}, $I_{\nabla\cdot\nabla}$, and I_{∇^2} denote the three terms above, respectively. The term $I_{\nabla\cdot\nabla}$ can be simplified by applying

$$f_i \nabla f_j^* = \tfrac{1}{2}\left[f_i \nabla f_j^* + \nabla(f_i f_j^*) - f_j^* \nabla f_i\right] \tag{3.6}$$

to each of the four factors. $I_{\nabla\cdot\nabla}$ then becomes

$$-\frac{1}{4}\left\langle \frac{(\Phi_i^* \nabla \Phi_j - \Phi_j \nabla \Phi_i^*) \cdot (J_i^* \nabla J_j - J_j \nabla J_i^*) + \nabla\left(\Phi_i^* \Phi_j\right) \cdot \nabla\left(J_i^* J_j\right)}{|\Psi_0|^2} \right\rangle_{|\Psi_0|^2} .$$

The expectation value $\langle Q \rangle_f$ is just $\int (fQ\, dR) / \int f\, dR$, and one can apply the first Green's transformation to the second term and write

$$\begin{aligned} -\frac{1}{4}\left\langle \frac{\nabla\left(\Phi_i^* \Phi_j\right) \cdot \nabla\left(J_i^* J_j\right)}{|\Psi_0|^2} \right\rangle_{|\Psi_0|^2} &= \frac{1}{4}\left\langle \frac{\Phi_i^* \Phi_j \cdot \nabla^2\left(J_i^* J_j\right)}{|\Psi_0|^2} \right\rangle_{|\Psi_0|^2} \\ = \frac{1}{4}\left\langle \frac{\Phi_i^* \Phi_j \cdot \left(J_i^* \nabla^2 J_j + J_j \nabla^2 J_i^* + 2 \nabla J_i^* \cdot \nabla J_j\right)}{|\Psi_0|^2} \right\rangle_{|\Psi_0|^2} , \end{aligned}$$

since the boundary terms vanish at infinity. The first two terms are now canceled by I_{∇^2}, and finally the original matrix element can be written as

$$\begin{aligned} H_{ij} =& \frac{1}{2}\left\langle \frac{J_i^* J_j \left(\Phi_i^* \mathsf{H} \Phi_j + \Phi_j \mathsf{H} \Phi_i^*\right)}{|\Psi_0|^2} \right\rangle_{|\Psi_0|^2} + \frac{1}{2}\left\langle \frac{\Phi_i^* \Phi_j \nabla J_i^* \cdot \nabla J_j}{|\Psi_0|^2} \right\rangle_{|\Psi_0|^2} \\ & - \frac{1}{4}\left\langle \frac{(\Phi_i^* \nabla \Phi_j - \Phi_j \nabla \Phi_i^*) \cdot (J_i^* \nabla J_j - J_j \nabla J_i^*)}{|\Psi_0|^2} \right\rangle_{|\Psi_0|^2} . \end{aligned} \tag{3.7}$$

If $J_i = J$ for all i, and J is real, then the last term becomes zero. Furthermore, if Φ_i's are the eigenfunctions of the (noninteracting) Hamiltonian, then the expression can be further simplified.

Chapter 4

Quantum Dots

In this thesis, two-dimensional semiconductor quantum dots are studied in various magnetic field strengths. Effective models are used for the semiconductor medium, but the correlated electrons confined by the dot potential are accurately modeled. The study in this chapter is restricted to two dimensions but, with a few exceptions, the generalization to three dimensions is straight-forward.

4.1 Models

The lateral size of even the smallest two-dimensional quantum dots is several tens of times larger than the lattice constant of the underlying lattice. Therefore, the effects of the lattice are modeled using the effective mass approximation, $m^* = m_\mathrm{r} m_0$, where m_0 is the electron's rest mass, m_r is a coefficient (relative mass) determined by the crystal structure, and m^* is the effective mass that replaces the rest mass in calculations. Likewise, electrostatic effects are described collectively by the effective permittivity, $\epsilon = \epsilon_\mathrm{r}\epsilon_0$, where ϵ_0 is the permittivity of vacuum, and ϵ_r the relative permittivity, and the Landé g-factor is replaced by the effective g-factor g^*. For electrons in GaAs, the values of these parameters are approximately $m_\mathrm{r} = 0.067$, ϵ_r =12.4–13.0, and $g^* = -0.44$ [33].

For single dots, the external potential V_ext is assumed to be symmetric and harmonic: $V_\mathrm{ext} = \frac{1}{2} m^* \omega_0^2 r^2$, where r is the distance from the center of the dot, and the parameter ω_0 determines the strength of the external confinement. The value of the confinement energy $\hbar\omega_0$ is typically in the meV range. The harmonic potential is a good approximation to the real potential,

and it is also analytically convenient. Much of the physical phenomena seen in experiments can be reproduced within the harmonic approximation [34], but in some cases, as in the far-infrared spectroscopy measurements, deviations from the harmonic potential become essential [35]. In any case, the harmonic potential can be used as a starting point in generating trial wave functions for other kinds of potentials.

For a negative charge q, the noninteracting single-particle Hamiltonian in magnetic field $\mathbf{B}$ is given by

$$\mathsf{H}_i = \frac{(\mathsf{p}_i - q_i\mathsf{A}_i)^2}{2m^*} + \tfrac{1}{2}m^*\omega_0^2\mathsf{r}_i^2 + \frac{g^*\mu_\mathrm{B}}{\hbar}\mathbf{B}\cdot\mathsf{s}_i\,, \tag{4.1}$$

where r and p are the position and momentum operators, respectively, and i is the particle index. A is the vector-potential operator ($\nabla\times\mathbf{A}=\mathbf{B}$), μ_B is the Bohr magneton, and s is the spin-angular-momentum operator. The Bohr magneton is the plain Bohr magneton ($\mu_\mathrm{B} = |q|\hbar/2m_0$ for an electron) because conventionally the effective mass is incorporated into the factor g^*.

The interaction Hamiltonian H_int is assumed to be purely Coulombic,

$$\mathsf{H}_\mathrm{int} = \sum_{i<j}\frac{q_iq_j}{4\pi\epsilon r_{ij}}\,, \tag{4.2}$$

where r_{ij} is the distance between particles i and j. Due to screening [36] and finite-thickness effects, other forms of the interaction are also justified. For example, the finite thickness of the dot softens the short-range part of the effective interaction potential.

4.1.1 Quantum dot molecules

For double dots with the separation d, the external potential is

$$V_\mathrm{ext}(x,y) = \tfrac{1}{2}m^*\omega_0^2\Big[\min\Big(x-\frac{d}{2},x+\frac{d}{2}\Big)^2 + y^2\Big]\,, \tag{4.3}$$

which, for $d=0$, reduces back to the single-quantum-dot potential. As $d\longrightarrow\infty$, the potential approaches that of two independent quantum dots. This system is studied in Publication III using the exact diagonalization.

4.2 Single-particle eigenstates

In a zero magnetic field, a harmonic quantum dot reduces to a two-dimensional harmonic oscillator. The potential is separable and has the usual

eigenfunctions, expressed using the Hermite polynomials in x and y directions as

$$\psi_{n,m} \propto H_n(x) H_m(y) \mathrm{e}^{-\frac{1}{2}(x^2+y^2)} \,, \tag{4.4}$$

where the coordinates are measured in units of $\sqrt{\hbar/m^*\omega_0}$. These functions are used for the single-particle states in Publication IV.

In a nonzero magnetic field the Hamiltonian (4.1) can still be solved analytically. For Coulomb gauges ($\nabla \cdot \mathbf{A} = 0$), the operators A and p commute with respect to the dot product. In the special case of the symmetric gauge, $\mathbf{A} = -\frac{1}{2}B\,(y\mathbf{i} - x\mathbf{j})$, one can further write $\mathsf{A} \cdot \mathsf{p} = \frac{1}{2}B\,\mathsf{l}_z$, where l_z is the z-component of the single-particle angular-momentum operator, and $\mathsf{A}^2 = \frac{1}{4}B^2\mathsf{r}^2$. In the symmetric gauge, the Hamiltonian (4.1) becomes

$$\begin{aligned} \mathsf{H} &= \frac{\mathsf{p}^2}{2m^*} + \frac{\mu_\mathrm{B}^*}{\hbar} B\,\mathsf{l}_z + \tfrac{1}{2}m^* \left(\frac{qB}{2m^*}\right)^2 \mathsf{r}^2 + \tfrac{1}{2}m^*\omega_0^2\mathsf{r}^2 + \frac{g^*\mu_\mathrm{B}}{\hbar} B\mathsf{s}_z \\ &= \frac{\mathsf{p}^2}{2m^*} + \tfrac{1}{2}m^* \left(\omega_0^2 + \tfrac{1}{4}{\omega_c}^2\right) \mathsf{r}^2 + \frac{\mu_\mathrm{B}^* B}{\hbar} \left(\mathsf{l}_z + \gamma^* \mathsf{s}_z\right) \,, \end{aligned} \tag{4.5}$$

where $\mu_\mathrm{B}^* = \mu_\mathrm{B}/m_\mathrm{r}$ is the effective Bohr magneton, $\omega_c = |q|B/m^*$ is the cyclotron frequency, and $\gamma^* = g^* m_\mathrm{r}$. The total confinement ω is defined as $\omega^2 = \omega_0^2 + \frac{1}{4}{\omega_c}^2$.

Switching to the coordinate representation and the effective harmonic oscillator (HO) unit system, which is obtained by setting $\hbar = m^* = |q| = \omega = 1$, the single-particle Hamiltonian can be written simply as

$$\mathsf{H} = -\tfrac{1}{2}\nabla^2 + \tfrac{1}{2}r^2 + \tfrac{1}{2}\omega_c \left(\mathsf{l}_z + \gamma^* \mathsf{s}_z\right) \,. \tag{4.6}$$

The coordinate part of the Hamiltonian (4.6) has the well-known Fock-Darwin [37] eigenfunctions, which in polar coordinates can be written as:

$$\psi_{n_L,l}(r,\theta) = C_{n_L,l}\; r^{|l|}\, \mathrm{e}^{\mathrm{i}l\theta}\, L_{n_L}^{(|l|)}(r^2)\, \exp\left(-\tfrac{1}{2}r^2\right) \,, \tag{4.7}$$

where $n_L \geq 0$ and $|l| \leq n_L$, $C_{n_L,l}$ is a normalization constant,

$$C_{n_L,l}^2 = \frac{n_L!}{\pi(n_L + |l|)!} \,, \tag{4.8}$$

and where $L_n^{(k)}$ is an associated Laguerre polynomial [38], defined by

$$\begin{aligned} (n+1)L_{n+1}^{(k)}(x) &= (2n + k + 1 - x)L_n^{(k)}(x) - (n+k)L_{n-1}^{(k)}(x) \,, \\ L_0^{(k)}(x) &= 1 \,, \quad \text{and} \\ L_1^{(k)}(x) &= 1 - x + k \,. \end{aligned} \tag{4.9}$$

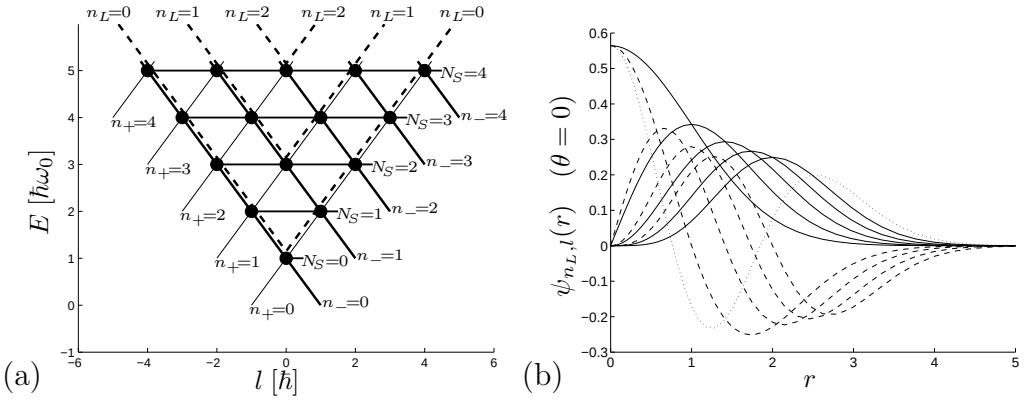

Figure 4.1: (a): Single-particle energy levels in a zero magnetic field. The indices used in this thesis are illustrated. For electrons, the states with a fixed n_- condense to form a Landau level when B is increased (see Fig. 4.2). (b): The radial part of the single-particle wave functions with $N_S \leq 4$. The solid lines are for $n_L = 0$, dashed for $n_L = 1$, and dotted for $n_L = 2$. Harmonic oscillator units are used.

The corresponding eigenenergies of the Hamiltonian (4.6) are

$$E_{n_L,l} = 1 + 2n_L + |l| + \tfrac{1}{2}\omega_c\,(l + \gamma^* s)\ , \tag{4.10}$$

where s is the spin quantum number. In a zero field, the states with the same $N_S = 2n_L + |l|$ are degenerate, and in an infinite field (in the positive z-direction, $\omega_c = +2$) the electron states with the same $n_- = n_L + \frac{1}{2}(|l| + l)$ and s are degenerate. Fig. 4.1 illustrates the various quantum numbers used, and the first few energies as functions of B are shown in Fig. 4.2.

In the sequel, the Zeeman term is neglected. The trial wave functions are eigenfunctions of the spin operator, and the Zeeman energy can always be added afterwards. For electrons in GaAs, the dimensionless factor γ^* in Eq. (4.10) is approximately -0.0295.

4.3 Many-particle states

For an interacting Hamiltonian, analytical many-particle eigenfunctions exist only for special forms of the interaction. For the Coulomb interaction,

$$\mathsf{H}_{\text{int}} = \sum_{i<j} \frac{C_{ij}}{r_{ij}}\,, \tag{4.11}$$

where C_{ij} is the interaction strength for pair ij, analytical solutions exists for

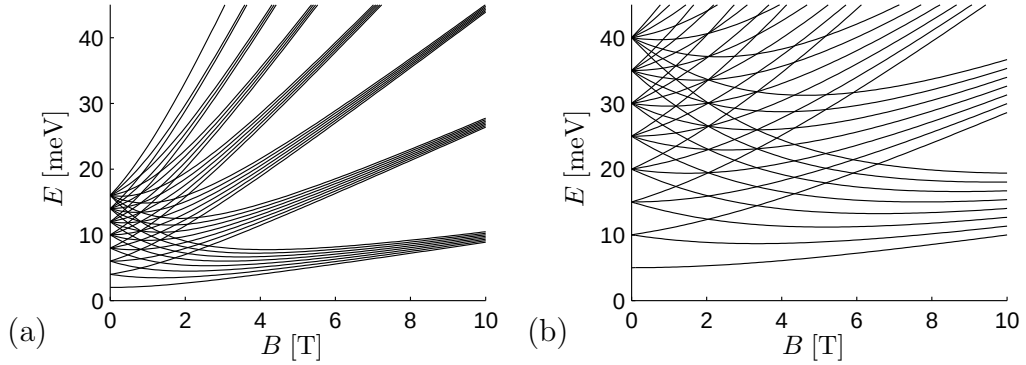

Figure 4.2: The single-particle energy levels [see Eq. (4.10)], without the Zeeman energy, as a function of the magnetic field for $m_{\mathrm{r}} = 0.067$, and confinement energies $\hbar\omega_0 = 2\,\mathrm{meV}$ (a) and $\hbar\omega_0 = 5\,\mathrm{meV}$ (b). The states with $N_S = 2n_L + |l| \leq 7$ are drawn. The Landau-level formation with increasing B is clearly visible.

two particles [39], but only for specific values of C. In the HO unit system, the interaction strength between two electrons has the value $C = \sqrt{\mathrm{Ha}^*/\hbar\omega}$, where Ha^* is the effective Hartree (see Sec. 4.6).

A widely used way to approximate interacting many-particle states is the Jastrow-Slater wave function:

$$\Psi = D_\uparrow D_\downarrow J\,, \tag{4.12}$$

where $D_{\uparrow(\downarrow)}$ is a Slater determinant for spin up (down) electrons, and the Jastrow factor J is a correlation factor depending on interparticle coordinates $\{\mathbf{r}_i - \mathbf{r}_j\}_{i<j}$ only. The wave function (4.12) is expected to be good if the interactions are weak, but with a stronger interaction strength the situation is more complicated. However, earlier it has been confirmed that the Jastrow factor can very efficiently capture the interaction effects [40–42] in small quantum dots. If Eq. (4.12) is not a sufficient approximation, a completely general many-electron wave function (with a given symmetry) can be written as the series

$$\Psi = \sum_{i,j} c_{i,j} D_\uparrow^{(i)} D_\downarrow^{(j)} J\,, \tag{4.13}$$

where $c_{i,j}$'s are complex coefficients, and $D^{(i)}$ is the ith determinant in some sequence of all possible Slater determinants with single-particle states from Eq. (4.7). The Jastrow factor J, in this case, has no profound significance; it merely accelerates the convergence of the summation.

The interaction energy in the HO unit system is proportional to $\omega^{-\frac{1}{2}}$. In the limit of a weak total confinement, i.e., small density, interactions begin to dominate over the kinetic energy, and the system is expected to reach a localized state [43–46]. The formation of this so-called Wigner-molecule state is studied in Publication IV.

By symmetry the (time-independent) many-particle wave functions are rotationally invariant. Therefore, from the charge density one cannot get information about the localization of particles. As proposed in Publication IV, a convenient tool to study the localization within the VMC scheme is the conditional probability

$$\tilde{\rho}(\mathbf{r}_1) \propto |\Psi(\mathbf{r}_1, \tilde{\mathbf{r}}_2, \ldots, \tilde{\mathbf{r}}_N)|^2 , \tag{4.14}$$

where the configuration $(\tilde{\mathbf{r}}_1, \ldots, \tilde{\mathbf{r}}_N)$ maximizes the probability density $|\Psi|^2$. The quantity $\tilde{\rho}$ has an analytical expression in the VMC scheme, and therefore, no statistical noise. This is an important difference from many other quantities, like the charge density. In Publication IV, contour plots of $\tilde{\rho}$ are given for a six-electron system.

4.3.1 Single-configuration states

If the Jastrow factor is set to unity in Eq. (4.12), the resulting wave function is an exact eigenstate of the noninteracting Hamiltonian with an eigenenergy equal to the sum of occupied single-particle energies. The local energy, including the interactions, can be written as

$$E_L^0 = \sum_i E_i + V_{\text{int}}^0 = E_{\text{const}} + V_{\text{int}}^0 , \tag{4.15}$$

where i enumerates the occupied single-particle states (n_L, l). The expectation value of the local energy reduces to

$$\left\langle E_L^0 \right\rangle_{|\Psi|^2} = E_{\text{const}} + \left\langle V_{\text{int}}^0 \right\rangle_{|\Psi|^2} . \tag{4.16}$$

All the system parameters are scaled away from the wave functions in Eq. (4.7) by switching to the effective harmonic oscillator unit system. Therefore, the matrix elements of a B-independent operator cannot depend on B. The Hamiltonian operator depends on B, but only through simple multiplicative factors [see Eqs (4.6) and (4.11)] to operators. As a result, the Hamiltonian matrix elements between single-configuration states can only

have a trivial B-dependence. As an example, in HO units the interaction energy for the state $\Psi = D$ is just

$$\left\langle V_{\text{int}}^0 \right\rangle_{|\Psi|^2} = C\, V_{\text{C}}^{\Psi}\,, \tag{4.17}$$

where V_{C}^{Ψ} is a constant for each state Ψ, and $C = C_{ij}$ is the common interaction strength between all electrons, depending on the magnetic field through $C = \sqrt{\text{Ha}^*/\hbar\omega}$ [see Eq. (4.11)].

4.3.2 Jastrow factor

The Jastrow factor J accounts for correlations. It can significantly lower the total energy and reduce its variance for high-density states. For electrons, the Jastrow factor creates a negative cusp to the wave function at $\mathbf{r}_i = \mathbf{r}_j$, and therefore keeps electrons further away from each other. This can be seen in Fig. 4.3. In this thesis the Jastrow factor also contains all the variational parameters.

In the presence of a Jastrow factor, let the different contributions to the total energy be defined by

$$\left\langle E_L^J \right\rangle_{|\Psi_J|^2} = \left\langle E_L^0 \right\rangle_{|\Psi_0|^2} + E_J + \Delta V_{\text{int}}\,, \tag{4.18}$$

where E_J is the difference in kinetic energies between states with and without the Jastrow factor, and ΔV_{int} is the corresponding difference in the potential energy. The expectation value $\left\langle E_L^J \right\rangle_{|\Psi_J|^2}$ now depends on B in a nontrivial way, because there is an explicit B-dependence in the Jastrow factor itself through cusp conditions. Fig. 4.4 illustrates this. A useful expression for E_J is given later in Eq. (4.37).

The form of the Jastrow factor is somewhat arbitrary, and several variants are used in the literature. In this thesis the Jastrow factor is of the form

$$J(\{\mathbf{r}_i\}) = \prod_{i<j} \exp\left(\frac{C_{ij} r_{ij}}{\beta_{ij} + \alpha_{ij} r_{ij}}\right)\,, \tag{4.19}$$

where α_{ij} is a variational parameter for the pair ij, and C_{ij} is the interaction strength. The parameters β_{ij} are fixed by the cusp conditions, as described in Sec. 2.4. By symmetry, only two parameters are free: $\alpha_{\uparrow\uparrow}$ for parallel spins and $\alpha_{\uparrow\downarrow}$ for antiparallel spins. The Jastrow factor (4.19) is an eigenfunction of the total-angular-momentum operator $\mathsf{L} = \sum_i \mathsf{l}_i$ with a zero eigenvalue, and as such it has no effect on the angular-momentum properties of Ψ.

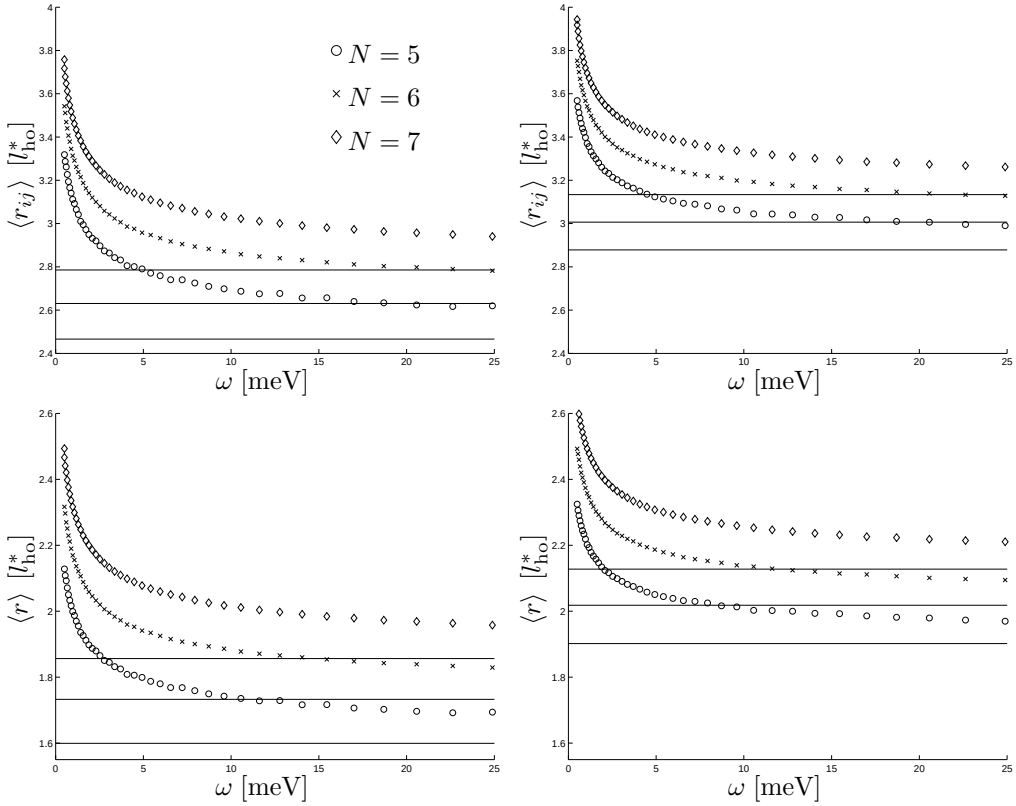

Figure 4.3: Upper row: the effect of the Jastrow factor on the interparticle separation for $N = 5, 6$, and 7 particles. On the left, the state is the first fully spin-polarized lowest-energy state (the MDD state, see Sec. 4.4.1) that appears when B is increased from zero. On the right, the state is the second fully spin-polarized lowest-energy state. The solid lines show the values for the corresponding states with $J = 1$, in the same order. The Jastrow factor increases the separation by creating a negative cusp to the wave function at $r_{ij} = 0$. Lower row: The effect on $\langle r_i \rangle$, where r_i is the distance of the ith particle from the origin, as a function of ω for the same states as above. All lengths are measured in $l^*_{\mathrm{ho}} = \sqrt{\hbar/m^*\omega}$.

As described in Sec. 2.2, the optimal values for parameters are found by minimizing the total energy. Because all the non-constant terms in Eqs (4.15) and (4.18), and also the wave function (4.12) itself, depend only on ω, it follows that for a given state, the optimal value of α, denoted α^*, is a function of ω only. In a few sample cases, Fig. 4.5 shows how the optimal value of $\alpha_{\uparrow\uparrow}$ depends on ω, and how the total energy depends on α.

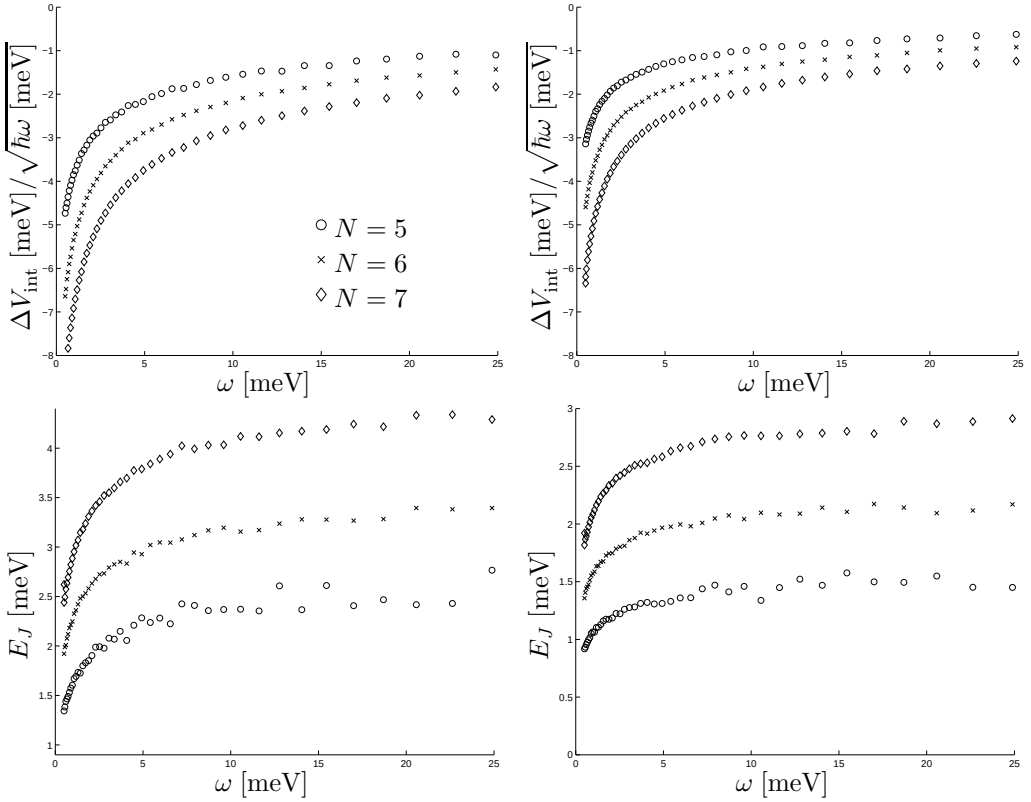

Figure 4.4: The effect of the Jastrow factor on the total energy for selected lowest-energy states for $N = 5, 6$, and 7 particles. Upper panels: the difference $\Delta V_{\rm int}$ in the potential energies between a state without a Jastrow factor, and the corresponding state with the Jastrow factor, scaled by $\sqrt{\hbar\omega/\rm meV}$ to remove the trivial $\sqrt{\omega}$ behavior. The states shown in the two panels are the same as in Fig. 4.3. Lower panels: the difference E_J in the kinetic energy as a function of ω for the same states as above. Corresponding curves from upper and lower panels together give the full Jastrow contribution to the total energy.

Also a linear Jastrow factor with no variational parameters,

$$J_{\rm lin}(\{r_{ij}\}) = \prod_{i<j}(1 + C_{ij}\beta_{ij}r_{ij})\,, \tag{4.20}$$

is tested in this thesis, but it does not improve upon the form (4.19).

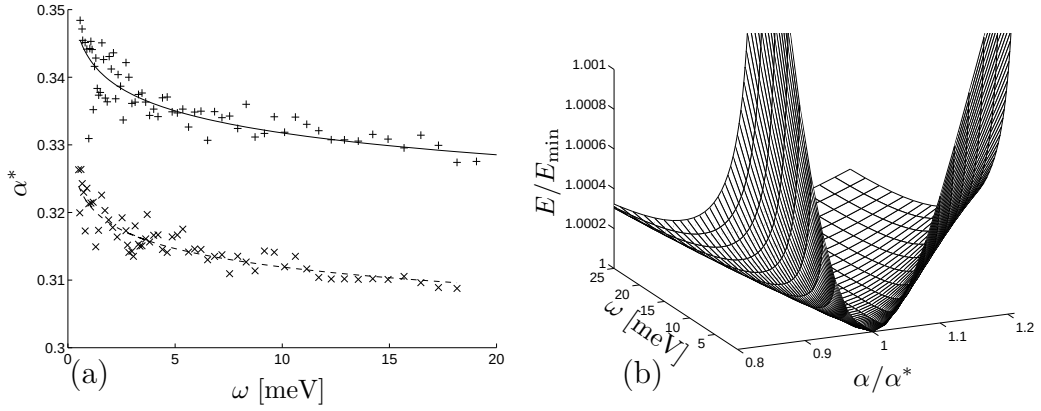

Figure 4.5: (a): The optimal Jastrow parameters α^* for two high-B six-particle states. The upper curve is for the first fully spin-polarized lowest-energy state, the MDD state (see Sec. 4.4.1), that appears when B is increased from zero, and the lower curve is the second fully spin-polarized lowest-energy state. For the MDD state, a power-law fit gives $\alpha^* = 0.32 \times \omega^{-0.013}$, and for the other state it gives $\alpha^* = 0.34 \times \omega^{-0.014}$. The parameters are in HO unit system: in an ω_c-independent unit systems the curves have an extra factor proportional to $\sqrt{\omega}$. (b): The relative energy $E/E_{\min}$ as a function of ω and the relative Jastrow parameter $\alpha/\alpha^*(\omega)$ for the six-electron MDD state. As $\omega \to 0$, the minimum in the parameter space becomes steeper.

4.3.3 Center-of-mass motion

For N particles, the center-of-mass coordinates $\{\tilde{\mathbf{r}}_i, \mathbf{r}_\mathrm{C}\}$ are defined as:

$$\begin{cases} \tilde{\mathbf{r}}_i = \mathbf{r}_i - \dfrac{1}{M}\displaystyle\sum_{j=1}^{N} m_j \mathbf{r}_j \\ \mathbf{r}_\mathrm{C} = \dfrac{1}{M}\displaystyle\sum_{j=1}^{N} m_j \mathbf{r}_j \end{cases} \qquad \Longleftrightarrow \qquad \mathbf{r}_i = \tilde{\mathbf{r}}_i + \mathbf{r}_\mathrm{C} \quad \left(\sum_i m_i \tilde{\mathbf{r}}_i = \mathbf{0} \right), \tag{4.21}$$

where $M = \sum m_i$. For the harmonic confinement (and constant $\mathbf{B}$) the center-of-mass motion is separable from relative coordinates:

$$\mathsf{H} = \sum_i \mathsf{H}_i + \mathsf{H}_\mathrm{int} = \mathsf{H}_\mathrm{C} + \sum_i \mathsf{H}'_i + \mathsf{H}_\mathrm{int}\,, \tag{4.22}$$

where H_C depends only on the center-of-mass coordinate $\mathbf{r}_\mathrm{C}$, and H'_i on the relative coordinates $\{\tilde{\mathbf{r}}_i = \mathbf{r}_i - \mathbf{r}_\mathrm{C}\}_i$, or equivalently, on coordinates

$\{\mathbf{r}_{ij} = \mathbf{r}_i - \mathbf{r}_j\}_{i<j}$. This implies any eigenstate of H to be of the form

$$\Psi = \Psi_{\mathrm{C}}(\mathbf{r}_{\mathrm{C}})\Psi_{\mathrm{r}}(\{\mathbf{r}_{ij}\})\,. \tag{4.23}$$

In any trial wave function for the ground state, the center-of-mass part should be restricted to be the lowest eigenstate of H_{C}. To guarantee this, the following coordinate transformation can be used:

$$z_k \to z_k - z_{\mathrm{C}} = \tilde{z}_k\,, \tag{4.24}$$

where z_k is the complex coordinate in the 2D plane, defined by $z_k = x_k + \mathrm{i}y_k$, and z_{C} is the corresponding complex center-of-mass coordinate. For the harmonic confinement this transformation is implicit in the relative part Ψ_{r} of all the wave functions presented in this thesis.

4.4 Many-particle states in a strong magnetic field

In an increasing magnetic field, the single-particle states condense (in energy) to discrete Landau levels[1] (see Fig. 4.2). As the magnetic field increases, the energy difference ΔE between states within one Landau level vanishes (in atomic or SI units) as $\Delta E \propto B^{-1}$, and the inter-level separation increases directly proportionally to B [see Fig. 4.2(b)]. If the magnetic field is strong enough, only the lowest Landau level (LLL) will be significant, because all the other levels are much higher in energy. This leads to the widely used LLL approximation, in which the many-body wave function is constructed from the LLL single-particle states only. In Publication VI it is shown that this approximation can lead to qualitative errors.

Relaxing the LLL approximation simply by including single-particle states from higher Landau levels is difficult. In strong fields, higher Landau levels also have a large density of states, and therefore no single state from a higher Landau level can have a dominating effect. In the case of the diagonalization (see Ch. 3), this leads to a quickly increasing number of basis functions. Also the analytical convenience given by the simple form of the LLL wave functions is lost by including states with $n_L \geq 1$.

In Publication VI, the effect of higher Landau levels is included into the total wave function through a Jastrow factor. It takes the wave function

[1]Some authors reserve the term "Landau level" strictly for the case $\omega_0 = 0$, and use the term "Fock-Darwin level" in the confined case $\omega_0 \neq 0$.

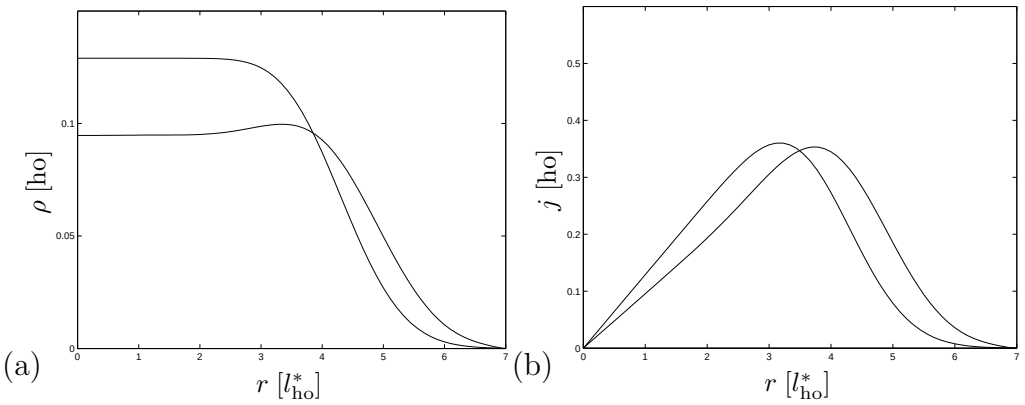

Figure 4.6: Total charge (a) and current (b) densities for a pure MDD state ($N = 8$) and the corresponding state with the Jastrow factor included. Densities that are shifted outward belong to the Jastrow case.

out of the LLL in an efficient way, yet preserving most of the analytical manageability. With the Jastrow factor taking care of the higher Landau levels, the problem of creating a good trial wave function is reduced back to the lowest Landau level.

4.4.1 Maximum-density-droplet state

For electrons, the states from Eq. (4.7) with a fixed $n_- = n_L + \frac{1}{2}(|l| + l)$ constitute a Landau level [see Fig.4.1(a)]. The lowest Landau level contains states with $n_- = 0$, i.e., $n_L = 0$ and $l \leq 0$. They have a simple form,

$$r^{|l|}\mathrm{e}^{\mathrm{i}l\theta}\exp\left(-\tfrac{1}{2}r^2\right) = z^{*|l|}\mathrm{e}^{-\frac{1}{2}r^2} = \varphi_l(x,y) \tag{4.25}$$

where $z = x + \mathrm{i}y$ is a complex coordinate in the two-dimensional plane, z^* is the complex conjugate of z, and $r^2 = x^2 + y^2$. The eigenenergies are

$$E_l = 1 + \left(\tfrac{1}{2}\omega_c - 1\right) l \qquad (l \leq 0)\,. \tag{4.26}$$

The N lowest (in energy) single-particle states from the LLL make up

the so-called maximum-density-droplet (MDD) wave function:

$$\Psi_{\mathrm{MDD}}(\{\mathbf{r}_i\}) = \begin{vmatrix} \varphi_0(\mathbf{r}_1) & \varphi_0(\mathbf{r}_2) & \cdots & \varphi_0(\mathbf{r}_N) \\ \varphi_1(\mathbf{r}_1) & \varphi_1(\mathbf{r}_2) & \cdots & \varphi_1(\mathbf{r}_N) \\ \vdots & \vdots & \ddots & \vdots \\ \varphi_{N-1}(\mathbf{r}_1) & \varphi_{N-1}(\mathbf{r}_2) & \cdots & \varphi_{N-1}(\mathbf{r}_N) \end{vmatrix} \tag{4.27}$$

$$= \prod_{i<j} \left(z_j^* - z_i^*\right) \, \exp\left(-\tfrac{1}{2}\sum_i r_i^2\right).$$

In the thermodynamical limit ($\omega_0 \to 0, N \to \infty$), this state corresponds to the $\nu = 1$ quantum-Hall state [1, 47], where ν is the filling fraction, i.e., the ratio between the density of electrons and the density of magnetic flux quanta. The MDD state has the total angular momentum $L_{\mathrm{MDD}} = -\frac{1}{2}N(N-1)$ and the energy $E_{\mathrm{MDD}} = N + \left(\frac{1}{2}\omega_c - 1\right) L_{\mathrm{MDD}}$. For a non-interacting, fully spin-polarized system, Ψ_{MDD} is the ground state in the limit of large B. Also for an interacting system Ψ_{MDD} is a decent approximation in a large range of magnetic field values, and it is the first fully spin-polarized state to appear as the magnetic field is increased from zero. Fig. 4.6 shows the charge and current-density profiles for the MDD state. In this thesis, the MDD state is a common factor in all trial states at high magnetic fields, even for the partially polarized ones.

4.4.2 Other fully spin-polarized states

As the magnetic field is increased, the total confinement ω increases and the electrons overlap more. To balance the increasing interaction energy, the system will at some point move to a new state with a lower angular momentum (higher in absolute value), $L = L_{\mathrm{MDD}} + \Delta L$ ($\Delta L < 0$), and a lower density. If the Zeeman factor is strong enough, the system will stay fully spin-polarized after the transition. In this case, ΔL can only take values from a set of "magic numbers" [7, 48].

A trial wave function for the fully spin-polarized state is of the form

$$\Psi_{\mathrm{D}} = DJ\,, \tag{4.28}$$

where D is a single determinant containing single-particle states from the lowest Landau level. Different many-particle states are constructed by occupying different single-particle states. Because the single-particle states are all from the LLL, the antisymmetric Ψ_{MDD} always factors out of D, leaving

$\Psi_{\rm D} = \Psi_{\rm MDD} J P_S^D$, where P_S^D is some polynomial, symmetric in variables z_i, and determined by the single-particle states in D. This suggests another form for the trial wave function:

$$\Psi_{\rm S} = \Psi_{\rm MDD} J P_S \,, \tag{4.29}$$

where P_S is any symmetric polynomial. This wave function can be written as a (finite) sum of terms like Eq. (4.28).

Both forms presented above can be used to construct bases for a given angular-momentum value. This is done in Sec. 4.5. Both sets of wave functions span the same Hilbert space, but the latter is often numerically easier to use. In Sec. 4.5.1 some properties of the latter wave function are derived.

4.4.3 Partially spin-polarized states

When the Zeeman coupling is weak, the system can re-enter a partially spin-polarized configuration even if the magnetic field is increased from the MDD region. This is studied in Publication VI, and the effects of higher Landau levels on transitions are examined.

As a trial wave function, a form similar to (4.29) is used:

$$\Psi_{\rm Y} = \Psi_{\rm MDD} J P \,. \tag{4.30}$$

The difference is that the polynomial P has a symmetry corresponding to the spin state, and in general is not symmetric in all variables. The polynomial can be constructed as follows:

$$\Psi_{\rm Y} = \mathcal{Y}_\chi \left(\Psi_{\rm MDD} J P^0 \right) = \Psi_{\rm MDD} J \, \mathcal{Y}'_\chi P^0 \,, \tag{4.31}$$

where χ is the number of inverted spins, $\mathcal{Y}_\chi$ is the Young's symmetrization operator, and $\mathcal{Y}'_\chi$ is the corresponding operator with the symmetrization and antisymmetrization directions interchanged. It is used because an antisymmetric factor $\Psi_{\rm MDD}$ is taken out of $\mathcal{Y}_\chi$. The polynomial P^0 is

$$P^0 = \prod_{i=1}^{|\Delta L|} z_i^* \,, \tag{4.32}$$

i.e., it brings ΔL units of additional angular momentum to the system. Then $\mathcal{Y}'_\chi P^0$ is just the required polynomial P in Eq. (4.30). The parameter χ determines the shape of the Young tableau corresponding to $\mathcal{Y}_\chi$.

Another, simpler trial wave function for the partially spin-polarized states is

$$\Psi_{\mathrm{J}} = D_\uparrow D_\downarrow J \prod_{\sigma_i \neq \sigma_j} (z_j^* - z_i^*)\,, \tag{4.33}$$

where σ_i is the spin of particle i, i.e., the product runs over antiparallel pairs of electrons. The single particle states $-l = 0, \ldots, N_\uparrow - 1$ are occupied in $D_\uparrow$, and states $-l = 1, \ldots, N_\downarrow$ in $D_\downarrow$. This state has the angular momentum $L = L_{\mathrm{MDD}} + \Delta L = L_{\mathrm{MDD}} - N_\downarrow$, and the spin $S = |N/2 + \Delta L|$, and as such it corresponds to the state $\Psi_{\mathrm{Y}}(\chi = N_\downarrow, \Delta L = N_\downarrow)$.

The reasoning behind both wave functions (4.31) and (4.33) is similar: with a given angular momentum and spin, it is advantageous to put the "free" zeros of the wave function on the opposite-spin electrons. The latter wave function does not have the correct symmetry, but gives surprisingly good energies. Because it is also fast to evaluate numerically, it is useful in some cases.

4.5 Bases for Monte Carlo diagonalization

As seen in the previous section, in strong magnetic fields the effects of higher Landau levels can be efficiently modeled using a Jastrow factor, and the rest of the wave function can be confined to the LLL. In this case, generating a suitable basis for an Monte Carlo diagonalization (MCD) is straightforward. In the MCD method the form of the trial wave functions is free, and an obvious choice for many-particle basis functions is found from Eq. (4.28):

$$\Psi_i = D_i J\,, \tag{4.34}$$

where D_i contains some (ith) set of single-particle states φ_l from the LLL ($l \leq 0$). Let Δl_j denote the (positive) integer representing the amount of additional angular momentum for state j in D, with respect to the MDD state, i.e., $\Delta l_j = |l_j| - j$ and $|\Delta L| = \sum_j \Delta l_j$. All the determinants corresponding to a given ΔL can now be enumerated by noting that the condition $|\Delta L| = \sum_j \Delta l_j$ gives a one-to-one correspondence between such determinants and the integer partitions[2] of the number $|\Delta L|$ with no more than N terms. Let $\boldsymbol{\lambda} = (\lambda_1, \lambda_2, \ldots, \lambda_N)$ be a partition of $|\Delta L|$ ($\lambda_i \geq 0$). The

[2]An (unrestricted) partition of an integer N is an ordered integer sequence $(n_1, n_2, \ldots, n_m)$ such that $n_i \geq n_{i+1}$ and $\sum_i n_i = N$. A k-restricted partition fulfills also $n_i \leq k$. The number of k-restricted partitions of N is the same as partitions of N with at most k terms; the two partition sets are conjugates of each other.

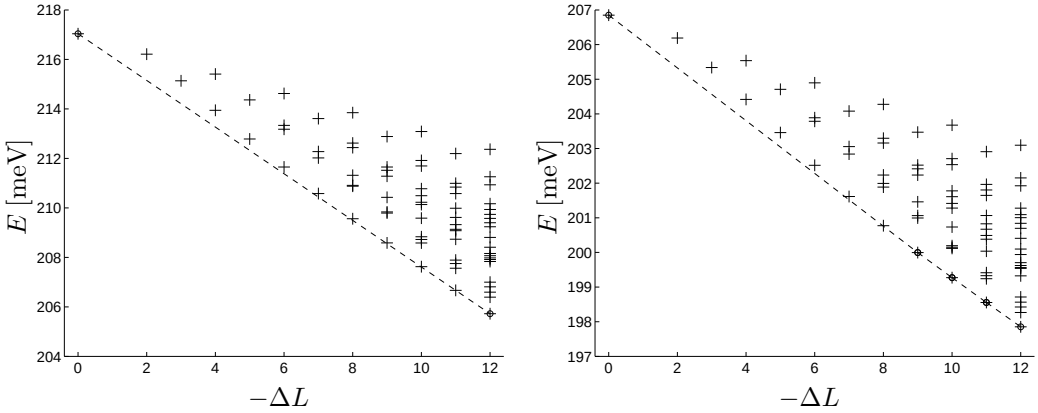

Figure 4.7: The spectrum of a 12-electron quantum dot in high magnetic field and a zero confinement for $|\Delta L| \leq 12$, computed using the MC diagonalization. Energies are only plotted at the lowest $|\Delta L|$-value they appear. Because $\omega_0 = 0$, every energy level appears also in the spectrum for higher $|\Delta L|$. The spectrum without the Jastrow factor is shown on the left, and on the right the Jastrow factor is included (the scales are different). Parameters are: $B = 5\,\mathrm{T}$, $\epsilon_\mathrm{r} = 13.0$, and $m_\mathrm{r} = 0.067$.

identification with determinants can be chosen to be $\Delta l_j = \lambda_{N-j+1}$, which is merely a rearrangement of the indices. Let $D(\boldsymbol{\lambda}) = D(\lambda_1, \lambda_2, \ldots, \lambda_N)$ denote this determinant.

Similarly as in Sec. 4.4.2, the determinant D_i can always be written as a product of Ψ_MDD and a symmetric polynomial. This gives again an alternate basis of the form

$$\Psi_i = \Psi_\mathrm{MDD} P_i J\,, \tag{4.35}$$

where P_i is a symmetric polynomial. This basis set is equivalent to the determinant basis [see Eq. (4.47)], but because Ψ_MDD is an explicit factor in *all* the basis functions, the latter set is far better than (4.34) for the MCD method. Figs 4.7 and 4.8 are produced using the MCD method with basis functions from Eq. (4.35). In Fig. 4.7 the full spectrum of a twelve-electron quantum dot is computed, and Fig. 4.8 shows the charge density of a quantum dot with an impurity.

With the basis $\Psi_i = \Phi_i J$, where $\Phi_i = \Psi_\mathrm{MDD} P_i$, and the driving wave function $\Psi_0 = \Psi_\mathrm{MDD} J$, the interacting Hamiltonian matrix element from

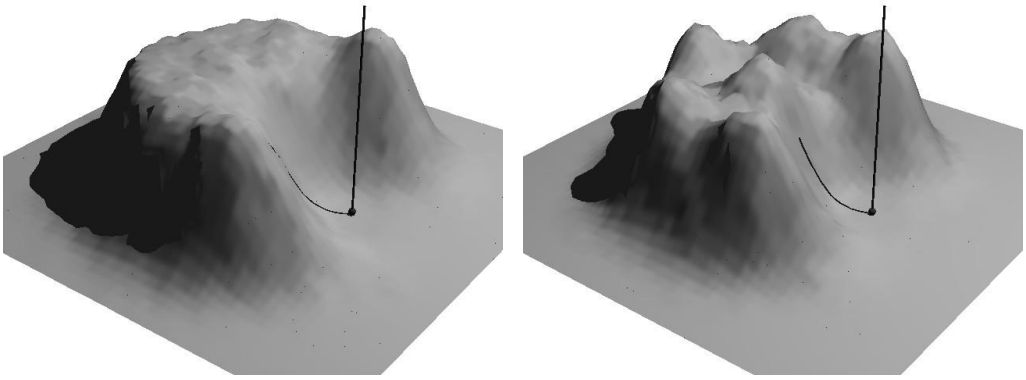

Figure 4.8: The charge density of a six-electron quantum dot, with point-like impurities (the charge $q_{\mathrm{imp}} = -|e|$) on the plane at the point indicated by the line segment. The magnetic field is 4 T on the left and 6 T on the right, and the external confinement is $\hbar\omega_0 = 3\,\mathrm{meV}$. The calculation used 227 basis functions with the MCD method.

Eq. (3.7) can be written simply as (here J is real)

$$\left\langle \frac{\Psi_i^* \mathsf{H} \Psi_j}{|\Psi_0|^2} \right\rangle_{|\Psi_0|^2} = \left\langle P_i^* \left(\tfrac{1}{2}\left(E_i + E_j\right) + V_{\mathrm{int}} + \frac{1}{2}\frac{\nabla J}{J} \cdot \frac{\nabla J}{J} \right) P_j \right\rangle_{|\Psi_0|^2} . \quad (4.36)$$

In the case of the traditional single-wave-function MC, the Jastrow (kinetic) energy term E_J in Eq. (4.18) and in Fig. 4.4 can therefore be expressed conveniently as

$$E_J = \tfrac{1}{2} \left\langle \left| \frac{\nabla J}{J} \right|^2 \right\rangle_{|\Psi|^2} = \tfrac{1}{2} \left\langle |\nabla \ln J|^2 \right\rangle_{|\Psi|^2} , \quad (4.37)$$

where Ψ is the trial wave function.

4.5.1 Symmetric polynomials

A function $f_{\mathrm{S}}(z_1, z_2, \ldots, z_N)$ is symmetric if it remains invariant under a permutation of arguments. Symmetric polynomials can be expressed in numerous different basis sets. Monomial polynomials, power sum polynomials, elementary symmetric polynomials, Schur polynomials, and complete polynomials can all be used to construct a basis for the space of symmetric polynomials [49,50]. Generally, any such basis function can be characterized by a vector of integers $\boldsymbol{\lambda} = (\lambda_1, \lambda_2, \ldots, \lambda_m)$.

The determinant basis presented above gives rise to the Schur polynomials $\sigma_{\boldsymbol{\lambda}}$:

$$D(\lambda_1, \lambda_2, \ldots, \lambda_N) = \Psi_{\mathrm{MDD}} \sigma_{\boldsymbol{\lambda}} \,. \tag{4.38}$$

Even though $\sigma_{\boldsymbol{\lambda}}$'s have a direct one-to-one correspondence to the noninteracting ground states, they are computationally unfavorable. A better choice for the basis is based on the elementary symmetric polynomials s_k. The basis constructed from them is also relatively diagonal with respect to the Hamiltonian, and the values of the polynomials and their derivatives can be evaluated extremely fast.

The kth-degree elementary symmetric polynomial, s_k, in N variables is defined as ($1 \leq k \leq N$):

$$s_k(z_1, z_2, \ldots, z_N) = \sum_{1 \leq i_1 < \cdots < i_k \leq N} z_{i_1} z_{i_2} \cdots z_{i_k} \;\; = \mathcal{S}_k z_1 z_2 \cdots z_k \,, \tag{4.39}$$

where $\mathcal{S}_k$ is the symmetrization operator in k indices (for N variables). The polynomials have $\binom{N}{k}$ terms, each of degree k. Every s_k is also linear in all the variables. The basis function $s_{\boldsymbol{\lambda}}$ is defined, using elementary symmetric polynomials, as a product (let us also define $s_0 = 1$)

$$s_{\boldsymbol{\lambda}} = \prod_k s_{\lambda_k} \,, \tag{4.40}$$

and the degree $d_{\boldsymbol{\lambda}}$ of $s_{\boldsymbol{\lambda}}$ is given by $d_{\boldsymbol{\lambda}} = \sum_k \lambda_k$. The vector $\boldsymbol{\lambda}$ can be identified to be a partition of the integer $d_{\boldsymbol{\lambda}}$.

The set $\{s_{\boldsymbol{\lambda}}\}$ forms a basis, and therefore any symmetric polynomial P can be written as a linear combination

$$P = \sum_i c_i s_{\boldsymbol{\lambda}_i} \,, \tag{4.41}$$

where c_i's are constants and $\{\boldsymbol{\lambda}_i\}$ is a set of vectors. As an example, $\sum_i z_i^3 = 3s_3 - 3s_1 s_2 + s_1^3$. For a polynomial P of degree M, the size of the basis is restricted by $d_{\boldsymbol{\lambda}_i} \leq M$ for all $\boldsymbol{\lambda}_i$. If P represents the symmetric polynomial part of a wave function that is an eigenstate of the angular momentum operator [see Eq. (4.29)], then all the terms in P must be of the same degree. In this case the restriction $d_{\boldsymbol{\lambda}} = M$ leads to a $P_M^{(N)}$-dimensional Hilbert space, where $P_M^{(N)}$ is the number of N-restricted integer partitions of M. There is no closed-form expression for $P_M^{(N)}$, but the Euler's recurrence relation [49] gives the number of unrestricted partitions, and Fig. 4.9 shows how $P_M^{(N)}$ behaves for small M and N.

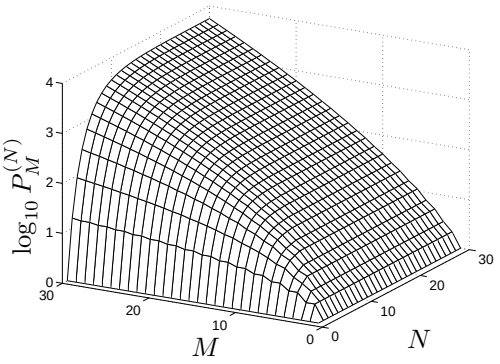

Figure 4.9: The logarithm of the number of N-restricted integer partitions of M. The asymptotic behavior in the unrestricted case ($N \geq M$) is $P_M \propto \exp(\sqrt{M})$.

Evaluation

In practice, Eq. (4.39) cannot be used to numerically evaluate s_k's. A quick algorithm based on the linearity of the elementary symmetric polynomials has been created [51] for the evaluation. Let us define $s_k^{(N)}$ to be s_k in all the N variables, and $s_k^{(N\setminus i)}$ to be s_k in variables other than z_i. The linearity can be used as follows:

$$s_k^{(N)} = s_k^{(N\setminus i)} + z_i s_{k-1}^{(N\setminus i)} \,. \tag{4.42}$$

This equation can be used to implement an algorithm to compute values of all s_i's, $1 \leq i \leq N$ in only $N(N-1)$ operations, using the memory space of input coordinate vector $(z_1, \ldots, z_N)$ only.

An algorithm to calculate the derivatives of the elementary symmetric polynomials has been developed in this thesis. The derivatives can be efficiently evaluated by using Eq. (4.42) twice. The algorithm is based on the following observation:

$$\frac{\partial}{\partial z_i} s_k^{(N)} = s_{k-1}^{(N\setminus i)} = s_{k-1}^{(N)} - z_i s_{k-2}^{(N\setminus i)} = s_{k-1}^{(N)} - z_i \frac{\partial}{\partial z_i} s_{k-1}^{(N)} \,. \tag{4.43}$$

The algorithm is recursive, but with a proper implementation the derivatives $\partial_i s_j$ for all $1 \leq i, j \leq N$ can be evaluated in only $2(N-1)^2$ operations, i.e., the cost is of the same order as the cost of evaluating s_k's themselves. The second and higher derivatives of s_k's are zero.

Conversions between bases

A symmetric polynomial written out in expanded form (in terms of variables z_i) is in monomial polynomial basis, i.e., the conversion to this basis from any other is trivial. The monomial polynomial $m_{\boldsymbol{\lambda}}$ can be defined as

$$m_{\boldsymbol{\lambda}} = \mathcal{S}_k z_1^{\lambda_1} z_2^{\lambda_2} \cdots z_k^{\lambda_k} \,, \tag{4.44}$$

where $\lambda_1 \geq \cdots \geq \lambda_k$. From $m_{\boldsymbol{\lambda}}$'s it is rather straightforward to switch to a power sum basis,

$$p_{\boldsymbol{\lambda}} = p_{\lambda_i} p_{\lambda_2} \cdots p_{\lambda_k} \,, \qquad \text{where} \quad p_k = \sum_i z_i^k \,. \tag{4.45}$$

The conversion between power sums and elementary polynomials can then be done using Newton-Girard formulae [52, Sec. 10.12] or the following determinant [53]:

$$p_k = \begin{vmatrix} s_1 & 1 & 0 & \cdots & 0 \\ 2s_2 & s_1 & 1 & \cdots & 0 \\ 3s_3 & s_2 & s_1 & \cdots & 0 \\ \vdots & \vdots & \ddots & \ddots & \vdots \\ ks_k & s_{k-1} & s_{k-2} & \cdots & s_1 \end{vmatrix} . \tag{4.46}$$

A helpful identification is the following: Let $\boldsymbol{\lambda}'$ be the conjugate partition of $\boldsymbol{\lambda}$. Then

$$s_{\boldsymbol{\lambda}} = \sigma_{\boldsymbol{\lambda}'} \quad + \text{terms from lower order partitions} \,. \tag{4.47}$$

A partition $\boldsymbol{\mu}$ is of lower order than $\boldsymbol{\lambda}$, if $\sum_{i=1}^{n} \mu_i \leq \sum_{i=1}^{n} \lambda_i$ for all n. For example,

$$D(1,1,1,1) = \Psi_{\mathrm{MDD}}\, s_4 \qquad \text{and} \qquad D(2,2,1,1) = \Psi_{\mathrm{MDD}}\, s_2 s_4$$

(in these cases no lower order terms are present). Eq. (4.47) also proves that bases (4.34) and (4.35) are equivalent.

4.6 Units

In this chapter effective harmonic oscillator units have been used, because in these units the eigenfunctions have a simple form. However, atomic units,

or effective atomic units are more widely used in mesoscopic physics. The former can be obtained by setting $\hbar = m = |q| = 4\pi\epsilon_0 = 1$, and latter by setting $\hbar = m^* = |q| = 4\pi\epsilon = 1$.

Let $E^*_{\mathrm{ho}} = \hbar\omega$ denote the unit energy of the effective harmonic oscillator unit system, and let E^*_{au} denote the unit energy of the effective atomic units, e.g. the effective Hartree Ha^*. The ratio between these two is

$$r = \frac{E^*_{\mathrm{au}}}{E^*_{\mathrm{ho}}} = \frac{\mathrm{Ha}^*}{\hbar\omega} = \frac{m^* q^4}{(4\pi\epsilon)^2\hbar^3\omega} \approx \frac{m_{\mathrm{r}}}{{\epsilon_{\mathrm{r}}}^2} \cdot \frac{27.21138345\,\mathrm{eV}}{\hbar\omega}\,. \tag{4.48}$$

Ratios between units of length and time in these unit systems can be expressed in terms of r:

$$\frac{l^*_{\mathrm{au}}}{l^*_{\mathrm{ho}}} = \frac{a^*_{\mathrm{B}}}{l^*_0} = r^{-\frac{1}{2}} \qquad \text{and} \qquad \frac{t^*_{\mathrm{au}}}{t^*_{\mathrm{ho}}} = r^{-1}\,. \tag{4.49}$$

Chapter 5

Results and conclusions

This thesis applies the exact wave function methods, variational quantum Monte Carlo (VMC) methods and the exact diagonalization method, to various quantum dot systems in a wide range of magnetic field values.

Publications I, II, and VI present results for states in high magnetic fields, i.e., post-MDD states. Publication I uses the Jastrow-Slater form for the spin-polarized wave function. The lowest-energy states in the range $\frac{1}{3} \leq \nu \leq 1$ are predicted, and compared to the composite fermion (CF) theory. Several cases are highlighted, in which the CF theory fails but the VMC approach gives correct lowest-energy states, which are compatible with exact-diagonalization studies. Transition points between the two first lowest-energy states are found to agree reasonably well with experiment. Publications II and VI study partially spin-polarized states in a high magnetic field, using a wave function with correct symmetry. The accuracy of the results is proven by comparison to exact-diagonalization results in Publication II. Publication VI produces phase diagrams of partially spin-polarized states for both lowest-Landau-level (LLL) states, and states with Landau-level-mixing (LLM) included. The effect of LLM is found to be significant, even in high magnetic fields in the post-MDD region. The study shows that LLM even suppresses the existence of certain spin-polarized states that normally appear as lowest-energy states in the widely used LLL approximation. It predicts that a state with a single spin flipped could be visible in experiments.

Publication IV is a study on the weak-confinement limit in a zero magnetic field. VMC method results are in excellent agreement with the most accurate numerical results available from diffusion and path-integral Monte Carlo calculations. The method is also applied in sufficiently low con-

finement in order to show a new, spin-polarized, low-density state. In an even weaker confinement, a smooth transition to a Wigner-molecule state is found. A conditional single-particle density is introduced and used to measure the localization of particles.

Publication III studies a two-electron quantum-dot molecule. It uses the exact diagonalization method and reveals an interesting spin-phase diagram, as a function of the interdot distance and the magnetic field. The states of the quantum-dot molecule are found to conform to the composite-fermion picture, even with surprisingly large interdot distances.

For Publication V a series of VMC calculations was performed in a wide range of magnetic field values, both for single and double quantum dots, to provide a benchmark results for density-functional-theory (DFT) methods. The agreement between different DFT methods and VMC is within the expected accuracy of DFT. Agreement is especially good for totally spin-polarized and spin-compensated cases.

As a general conclusion, the VMC method proves to be an accurate and efficient tool to study highly correlated electron systems. Results are accurate for the systems studied, even with relatively simple trial wave functions, and the computational cost to obtain satisfactory results is low compared to other techniques. Furthermore, since the actual wave functions are available in VMC, many physical quantities can be studied that are unavailable in some other techniques.

The Monte Carlo-based diagonalization method, which is developed in this thesis, combines the exact diagonalization and traditional quantum Monte Carlo methods. It can be used to study geometries that have no obvious trial wave function, for example, symmetry-broken ones. It can also be used to study excited states within the VMC scheme and can be expected to have diverse applications.

Bibliography

[1] K. v. Klitzing, G. Dorda, and M. Pepper. Phys. Rev. Lett. **45**, 494 (1980).

[2] D. C. Tsui, H. L. Stormer, and A. C. Gossard. Phys. Rev. Lett. **48**, 1559 (1982).

[3] H. L. Stormer, D. C. Tsui, and A. C. Gossard. Rev. Mod. Phys. **71**, S298 (1999).

[4] R. O. Jones and O. Gunnarsson. Rev. Mod. Phys. **61**, 689 (1989).

[5] W. M. C. Foulkes, L. Mitas, R. J. Needs, and G. Rajagopal. Rev. Mod. Phys. **73**, 33 (2001).

[6] S. Tarucha, D. G. Augustin, T. Honda, R. J. van der Hage, and L. P. Kouwenhoven. Phys. Rev. Lett. **77**, 3613 (1996).

[7] L. P. Kouwenhoven, T. H. Oosterkamp, M. W. S. Danoesastro, M. Eto, D. G. Austing, T. Honda, and S. Tarucha. Science **278**, 1788 (1997). In Reports.

[8] J. D. Thomson, H. D. Summers, P. M. Smowton, E. Herrmann, and P. Blood. J. Appl. Phys **90**, 4859 (2001).

[9] C. Ribbat, R. L. Sellin, I. Kaiander, F. Hopfer, N. N. Ledentsov, D. Bimberg, A. R. Kovsh, V. M. Ustinov, A. E. Zhukov, and M. V. Maximov. Appl. Phys. Lett. **82**, 952 (2003).

[10] S. Komiyama, O. Astafiev, V. Antonov, T. Kutsuwa, and H. Hirai. Nature **403**, 405 (2000).

[11] S. Cortez, O. Krebs, S. Laurent, M. Senes, X. Marie, P. Voisin, R. Ferreira, G. Bastard, J.-M. Gérard, and T. Amand. Phys. Rev. Lett. **89**, 207401 (2002).

[12] A. Ekert and R. Jozsa. Rev. Mod. Phys. **68**, 733 (1996).

[13] A. Galindo and M. A. Martín-Delgado. Rev. Mod. Phys. **74**, 347 (2002).

[14] H. Brune, M. Giovannini, K. Bromann, and K. Kern. Nature **394**, 451 (1998).

[15] V. A. Shchukin and D. Bimberg. Rev. Mod. Phys. **71**, 1125 (1999).

[16] P. M. Petroff, A. Lorke, and A. Imamoglu. Physics Today **54**, 46 (2001).

[17] P. Jensen. Rev. Mod. Phys. **71**, 1695 (1999).

[18] L. Kouwenhoven and C. Marcus. Physics World (1998).

[19] M. A. Reed, J. N. Randall, R. J. Aggarwal, R. J. Matyi, T. M. Moore, and A. E. Wetsel. Phys. Rev. Lett. **60**, 535 (1988).

[20] L. P. Kouwenhoven, A. T. Johnson, N. C. van der Vaart, C. J. P. M. Harmans, and C. T. Foxon. Phys. Rev. Lett. **67**, 1626 (1991).

[21] S. Ulam, R. D. Richtmeyer, and J. von Neumann. *Statistical methods in neutron diffusion*. Technical Report LAMS-551, Los Alamos National Laboratory (1947).

[22] N. Metropolis and S. Ulam. J. Am. Stat. Assoc. **44**, 335 (1949).

[23] N. Metropolis, A. W. Rosenbluth, M. N. Rosenbluth, A. H. Teller, and E. Teller. J. Chem. Phys. **21**, 1087 (1953).

[24] P. R. C. Kent, R. J. Needs, and G. Rajagopal. Physical Review B **59**, 12344 (1999).

[25] D. Bressanini and G. Morosi. J. Chem. Phys. **116**, 5345 (2002).

[26] A. Harju, B. Barbiellini, S. Siljamäki, R. M. Nieminen, and G. Ortiz. Phys. Rev. Lett. **79**, 1173 (1997).

[27] P. Young. In *Optimization in Action*, edited by L. C. W. Dixon. Institute of Mathematics and its Applications (Academic Press, London, 1976), pp. 517–573.

[28] X. Lin, H. Zhang, and A. M. Rappe. J. Chem. Phys. **112**, 2650 (2000).

[29] T. Kato. Comm. Pure Appl. Math. **10**, 151 (1957).

[30] E. A. Hylleraas and B. Undheim. Z. Phys **65**, 759 (1930).

[31] J. K. L. MacDonald. Phys. Rev. **43**, 830 (1933).

[32] L. D. A. Siebbeles and C. L. Sech. J. Phys. B: At. Mol. Opt. Phys. **27**, 4443 (1994).

[33] C. Weisbuch and C. Hermann. Physical Review B **15**, 816 (1977).

[34] N. A. Bruce and P. A. Maksym. Physical Review B **61**, 4718 (2000).

[35] D. Pfannkuche and R. R. Gerhardts. Physical Review B **44**, 13132 (1991).

[36] L. D. Hallam, J. Weis, and P. A. Maksym. Physical Review B **53**, 1452 (1996).

[37] V. Fock. Z. Phys. **61**, 126 (1930).

[38] G. Arfken. *Mathematical Methods for Physicists* (Academic Press, Inc., San Diego, 1985), third edition.

[39] M. Taut. J. Phys. A **27**, 1045 (1994).

[40] A. Harju, V. A. Sverdlov, and R. M. Nieminen. Europhys. Lett. **41**, 407 (1998).

[41] A. Harju, V. A. Sverdlov, B. Barbiellini, and R. M. Nieminen. Physica B **255**, 145 (1998).

[42] A. Harju, V. A. Sverdlov, R. M. Nieminen, and V. Halonen. Physical Review B **59**, 5622 (1999).

[43] E. Wigner. Phys. Rev. **46**, 1002 (1934).

[44] B. Tanatar and D. M. Ceperley. Physical Review B **39**, 5005 (1989).

[45] E. Goldmann and S. R. Renn. Physical Review B **60**, 16611 (1999).

[46] E. Räsänen, H. Saarikoski, M. J. Puska, and R. M. Nieminen. Physical Review B **67**, 035326 (2003).

[47] R. B. Laughlin. Physical Review B **23**, 5632 (1981).

[48] P. A. Maksym and T. Chakraborty. Physical Review B **45**, 1947 (1992).

[49] I. G. Macdonald. *Symmetric Polynomials and Hall Functions* (Oxford University Press, New York, 1995), second edition.

[50] E. Mukhin. Symmetric polynomials and partitions. Unpublished.

[51] S. Siljamäki. *Quantum Monte Carlo Calculations of a Few Electron Quantum Dots in High Magnetic Field*. Master's thesis, Helsinki University of Technology (1999).

[52] R. Séroul. *Programming for Mathematicians* (Springer, Berlin, 2000).

[53] J. Littlewood. *A University Algebra* (Heinemann, London, 1958), second edition.